AEDC-TR-76-6
AFATL-TR-75-164

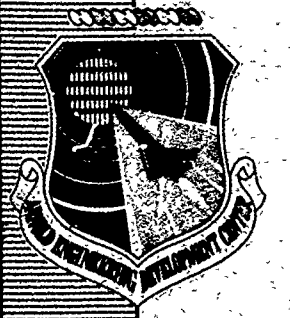

A WIND TUNNEL INVESTIGATION OF IMPULSE EFFECTS ON THE MOTION OF AN IMPULSE CORRECTION GUIDANCE MISSILE

VON KÁRMÁN GAS DYNAMICS FACILITY
ARNOLD ENGINEERING DEVELOPMENT CENTER
AIR FORCE SYSTEMS COMMAND
ARNOLD AIR FORCE STATION, TENNESSEE 37389

April 1976

Final Report for Period – July 24, 1975

Approved for public release; distribution unlimited.

Prepared for

AIR FORCE ARMAMENT LABORATORY (DLDL)
EGLIN AIR FORCE BASE, FLORIDA 32542

DISCLAIMER NOTICE

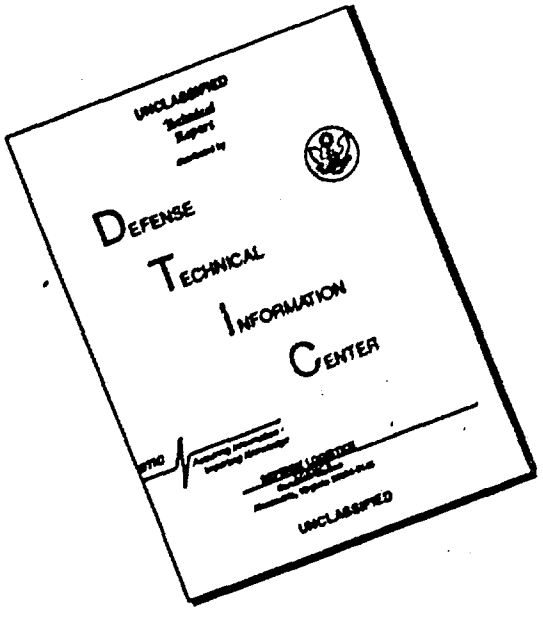

THIS DOCUMENT IS BEST QUALITY AVAILABLE. THE COPY FURNISHED TO DTIC CONTAINED A SIGNIFICANT NUMBER OF PAGES WHICH DO NOT REPRODUCE LEGIBLY.

NOTICES

When U. S. Government drawings specifications, or other data are used for any purpose other than a definitely related Government procurement operation, the Government thereby incurs no responsibility nor any obligation whatsoever, and the fact that the Government may have formulated, furnished, or in any way supplied the said drawings, specifications, or other data, is not to be regarded by implication or otherwise, or in any manner licensing the holder or any other person or corporation, or conveying any rights or permission to manufacture, use, or sell any patented invention that may in any way be related thereto.

Qualified users may obtain copies of this report from the Defense Documentation Center.

References to named commercial products in this report are not to be considered in any sense as an endorsement of the product by the United States Air Force or the Government.

This report has been reviewed by the Information Office (OI) and is releasable to the National Technical Information Service (NTIS). At NTIS, it will be available to the general public, including foreign nations.

APPROVAL STATEMENT

This technical report has been reviewed and is approved for publication.

FOR THE COMMANDER

Carl J. Schulze

CARL J. SCHULZE
Major, USAF
Chief Air Force Test Director, VKF
Directorate of Test

Craig E. Mahaffy

CRAIG E. MAHAFFY
Colonel, USAF
Director of Test

REPORT DOCUMENTATION PAGE

READ INSTRUCTIONS BEFORE COMPLETING FORM

1. REPORT NUMBER: AEDC-TR-76-6 / AFATL-TR-75-164
2. GOVT ACCESSION NO.
3. RECIPIENT'S CATALOG NUMBER
4. TITLE (and Subtitle): A WIND TUNNEL INVESTIGATION OF IMPULSE EFFECTS ON THE MOTION OF AN IMPULSE CORRECTION GUIDANCE MISSILE
5. TYPE OF REPORT & PERIOD COVERED: Final Report - July 24, 1975
6. PERFORMING ORG. REPORT NUMBER
7. AUTHOR(s): Bob L. Uselton - ARO, Inc.
8. CONTRACT OR GRANT NUMBER(s): AF-2547, ARO-V41A-94A
9. PERFORMING ORGANIZATION NAME AND ADDRESS: Arnold Engineering Development Center (XO), Air Force Systems Command, Arnold Air Force Station, Tennessee 37389
10. PROGRAM ELEMENT, PROJECT, TASK AREA & WORK UNIT NUMBERS: Program Element 62602F, Project 2547
11. CONTROLLING OFFICE NAME AND ADDRESS: Air Force Armament Laboratory (DLDL), Eglin Air Force Base, Florida 32542
12. REPORT DATE: Apr[redacted]76
13. NUMBER OF PAGES: 45
14. MONITORING AGENCY NAME & ADDRESS (if different from Controlling Office): AFATL; TR-75-164; 47 p.
15. SECURITY CLASS. (of this report): UNCLASSIFIED
15a. DECLASSIFICATION/DOWNGRADING SCHEDULE: N/A
16. DISTRIBUTION STATEMENT (of this Report)

Approved for public release; distribution unlimited.

17. DISTRIBUTION STATEMENT (of the abstract entered in Block 20, if different from Report)
18. SUPPLEMENTARY NOTES

Available in DDC

19. KEY WORDS (Continue on reverse side if necessary and identify by block number)

air to surface missiles
guidance
supersonic flow
angle of attack
Reynolds number
wind tunnel models

20. ABSTRACT (Continue on reverse side if necessary and identify by block number)

Wind tunnel tests were conducted for the Air Force Armament Laboratory to obtain experimental data at Mach number 3 on an impulse correction guidance system. The guidance system is based on the principle of impulse correction. The purpose of the test program was to determine if the interaction of the impulse explosion with the supersonic airflow caused an effect on the model motion. The small-amplitude free-oscillation

DD FORM 1 JAN 73 1473 EDITION OF 1 NOV 65 IS OBSOLETE

042 550

20. ABSTRACT (Continued)

technique was used to obtain data on a 0.5 scale model at angles of attack from 1 to 4.4 deg at Reynolds numbers, based on model length, of 12.2 x 10^6 and 23.1 x 10^6. The explosion which produced the impulse affected the model flow field. However, this perturbed flow field did not produce any significant effects on the model motion, apparently because of the short action time involved.

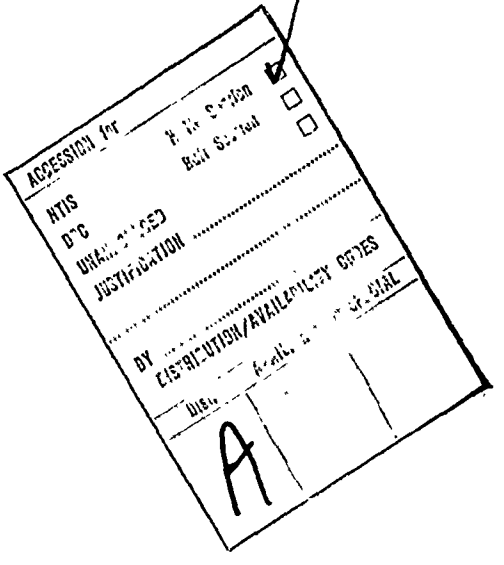

AFSC
Arnold AFS Tenn

PREFACE

The work reported herein was conducted by the Arnold Engineering Development Center (AEDC), Air Force Systems Command (AFSC) for the Air Force Armament Laboratory (AFATL) under Program Element 62602F, Project 2547. The AFATL project monitor was Mr. Kenneth Cobb. The results presented herein were obtained by ARO, Inc. (a subsidiary of Sverdrup & Parcel and Associates, Inc.), contract operator of AEDC, AFSC, Arnold Air Force Station, Tennessee. The test was done under ARO Project No. V41A-94A. The author of this report was Bob L. Uselton, ARO, Inc. The final data package was completed on September 5, 1975, and the manuscript (ARO Control No. VKF-TR-75-155) was submitted for publication on October 30, 1975.

CONTENTS

ILLUSTRATIONS

Figure

TABLES

1.0 INTRODUCTION

The Air Force Armament Laboratory (AFATL) is considering a guidance system which is based on impulse correction. An explosive strip is detonated forward of the rocket center of gravity and flight correction is obtained through the impulse acting on the center of gravity and lift from the moment-induced angle of attack. The action time of the explosive strip thruster is on the order of 10^{-4} seconds. This guidance technique is considered promising since it is relatively simple and cheap as compared with the methods currently used.

Investigations on the effectiveness of the impulse corrections to the flight path were conducted by AFATL using computer simulations. These studies, which assumed there was no interaction of the explosion with the missile aerodynamics, indicated that the system should perform satisfactorily. The purpose of the present test program at the Arnold Engineering Development Center (AEDC) von Karman Gas Dynamics Facility (VKF) was to determine if the interaction of the explosion with the supersonic airflow caused an effect on the model motion. The effect could be an amplitude amplification similar to that caused by a lateral jet (Ref. 1) or a delayed reaction of the perturbed flow field with the tail fins. The free oscillation cross flexure technique was utilized to measure the motion produced by the impulse and also model aerodynamic stiffness and damping. To assess the impulse effect, the measured motion was compared with interaction-free motion calculated from an analytical model. Wind tunnel tests were conducted at Mach number 3, and data were obtained at angles of attack from 1 to 4.4 deg at Reynolds numbers, based on model length, of 12.2×10^6 and 23.1×10^6.

2.0 APPARATUS

2.1 MODEL

The model (Fig. 1) was designed and fabricated at VKF with the exception of the design of the nose slots for

the impulse charges. Aerojet Solid Propulsion Company was subcontracted by AEDC to design the model nose slots and to select, size, and supply the detonators, explosive charges, and the charge covers. The nose section (47.7 percent of model length) was fabricated from 17-4 PH stainless steel while the body (52.3 percent of model length) was fabricated from aluminum for ballast purposes. Basically the model had a blunt nose, a 2-in.-diam cylindrical body, four rectangular tail fins, and a length of 40.5 in. The moment reference point and model pivot axis were located 13.329 in. ($x_p/\ell = 0.329$) from the model nose. The model was balanced to locate the center of gravity on the model pivot axis.

The explosive material (Dupont-Detasheet-C®), detonators, and plexiglasss covers are shown in Fig. 2. The explosive was bonded to the plexiglass cover which was then mounted in the model nose slot (Fig. 3) above the detonator and was held in place by nylon screws. However, metal screws were used for the cover installation photograph (Fig. 4). The explosion would disintegrate the covers and the heads of the nylon screws. Nonmetallic covers and screws were used to decrease the possibility of damage to the tunnel windows and floor. Two model noses were fabricated so that an explosive charge could be installed in one nose while the other nose was being tested in the wind tunnel. Each model nose contained six forward and six aft slots (Fig. 3) for the impulse charges. In future discussions in this report, the location of the explosive charge will be referred to as forward or aft impulse. Six slots in each section were fabricated because it was thought that repeated explosions in the same slot would deteriorate the slot edges which in turn would affect the repeatability of the impulse. However, Aerojet laboratory tests, conducted after completion of the model nose fabrication, showed that 20 of the present size explosives could be detonated in one slot without deteriorating the slot edges. Model details are shown in Fig. 5.

2.2 BALLISTIC PENDULUM

Four impulse levels dependent on balance angular limit, balance and aerodynamic stiffness, and configuration were required for the test program. The impulses were scaled to

produce an initial peak amplitude of 1.2 deg for the tunnel tests and 1.5 and 1.8 deg for VKF laboratory tests (wind-offs). Aerojet selected the ballistic pendulum to determine the explosive configuration required to produce the desired impulse levels. The pendulum weight was fabricated from the same material as the model nose (17-PH stainless steel), and both pieces of material had the same heat treatment specifications. This allowed assessment of the effects of the explosive on the slot edges as discussed in Section 2.1. The model slot designs (forward and aft) were machined on the pendulum weight, one on each side. The pendulum weight was supported by a rod which was inserted in a pivot housing. The housing was supported by bearings, and an angular transducer was used to measure the angular deflection due to the impulse. The output of the angular transducer was recorded by an oscillograph and was used to determine the amplitude and period of oscillation which are proportional to the impulse as can be seen in Section 4.1. The pendulum system was installed in a vacuum tank which allowed testing at atmospheric and vacuum conditions.

2.3 TEST MECHANISM AND INSTRUMENTATION

The VKF 2.G high-alpha pitch-damping test mechanism (Ref. 2, Fig. 6) was used to measure the model motion resulting from the impulse and to obtain pitch-damping data. The test mechanism utilizes a small-amplitude one-degree-of-freedom cross-flexure balance which is supported by a strut and sting. A strain-gage bridge is located on the flexures to provide a voltage proportional to angular displacement. A pneumatic- and spring-operated locking device is provided to hold the model during injection into or retraction from the tunnel. Three balances, having flexure stiffnesses of 2.3, 23, and 49 in.-lb/deg and maximum amplitudes of ±4, ±3, and ±2 deg, respectively, are available for use with the test mechanism. The 49-in.-lb/deg balance was used during the present test. An installation photograph is shown in Fig. 7.

The pitch-damping data were obtained utilizing an oscillating-air system to displace the model. The driving force was obtained from a high-pressure air supply which was adjusted to the pressure level necessary to overcome the damping moment. The model was oscillated by an air jet (Fig. 7) that was regulated by a remotely controlled servovalve oscillating at the natural frequency of the model-balance system. The driving force could be stopped

abruptly by a solenoid valve and data recorded as the amplitude decreased. During the impulse tests, the oscillatory model motion resulting from the impulse was recorded.

2.4 WIND TUNNEL

Tunnel A (Fig. 8) is a continuous, closed-circuit, variable density wind tunnel with an automatically driven flexible-plate-type nozzle and a 40- by 40-in. test section. The tunnel can be operated at Mach numbers from 1.5 to 6 at maximum stagnation pressures from 29 to 200 psia, respectively, and stagnation temperatures up to 750°R ($M_\infty = 6$). Minimum operating pressures range from about one-tenth to one-twentieth of the maximum at each Mach number. The tunnel is equipped with a model injection system which allows removal of the model from the test section while the tunnel remains in operation.

3.0 TEST CONDITIONS AND PROCEDURE

3.1 TEST CONDITIONS

The nominal wind tunnel test parameters at which the data were obtained are presented in Table 1.

3.2 TEST PROCEDURE

3.2.1 Pitch-Damping Data

The test procedure was to set the forcing air pressure to a sufficiently high value, open the solenoid valve, adjust the frequency of the servovalve to the natural frequency of the model-balance system, and then, when the model amplitude reached the desired value, close the solenoid valve. The switch that closed the valve also started the high-speed scanner which read the digitized angular position (θ) signal onto the magnetic tape for data reduction. Data reduction was accomplished by the logarithm decrement method described in Ref. 3.

3.2.2 Impulse Data

The test procedure was to load the detonator in the model nose, put the nose on the aft portion of the model, and then install the explosive and plexiglass cover. An electronic control circuit which incorporated three

safety interlocks was used to correlate the explosion with the data system and high-speed (7,500 frames/sec) schlieren motion pictures. After the explosive was loaded, the sequence of events was: (1) analog tape was manually started, (2) when the analog tape was up to speed, the schlieren motion-picture camera automatically started, (3) when the schlieren motion-picture camera was up to speed, the high-speed scanner data system was automatically started, (4) detonation. The high-speed scanner recorded the model motion (digitized angular position signal) onto magnetic tape for data reduction, and the high-speed schlieren motion pictures recorded the explosion and the effects on the model flow field.

4.0 DATA REDUCTION AND PRECISION OF DATA

4.1 AEROJET LABORATORY TESTS

Aerojet used the following equations to calculate the impulse produced by the ballistic pendulum.

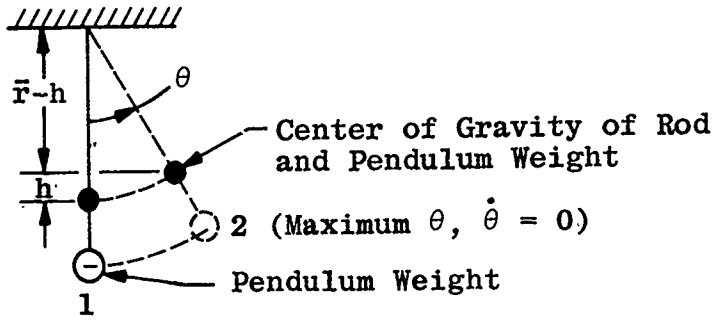

Sketch A

Since the action time of the explosion (t_1) is very small, it is assumed that the pendulum does not move during this time interval. With the pendulum initially at rest (t = 0),

$$[\text{Kinetic Energy}]_1 = [\text{Potential Energy}]_2$$

$$\tfrac{1}{2}I\dot{\theta}_1^2 = mgh$$

$$\dot{\theta}_1^2 = 2mg\bar{r}(1 - \cos\theta_2)/I$$

$$I = k^2m$$

$$\dot{\theta}_1 = 1/k[2g\bar{r}(1 - \cos\theta_2)]^{\frac{1}{2}} \qquad (1)$$

then

$$\text{Angular Impulse} = \text{Change in Angular Momentum}$$

$$r\int_0^{t_1} F\,dt = I(\dot{\theta}_1 - \dot{\theta}_0)$$

$$\dot{\theta}_0 = 0$$

$$\text{Impulse} = I\dot{\theta}_1/r$$

$$\text{Impulse} = \frac{k^2 m\dot{\theta}_1}{r}$$

By substituting for $\dot{\theta}_1$ from Eq. (1),

$$\text{Impulse} = \frac{km}{r}\,[2g\bar{r}(1 - \cos\theta_2)]^{\frac{1}{2}}$$

$$\text{Impulse} = \left(\frac{2Wk}{gr}\right)[g\bar{r}]^{\frac{1}{2}}\,[\sin(\theta_2/2)] \qquad (2)$$

The amplitude (θ_2) and period of oscillation were obtained from the output of the angular transducer. The radius of gyration (k) can be calculated, using the period of oscillation, and the weight (W), the distance to the point of action of the explosion (r), and the distance to center of gravity of the system ($\bar{r}$), are all measurable quantities. Therefore, all quantities on the right hand side of Eq. (2) are known and the impulse due to the explosive strip can be simply calculated.

In sizing the four impulse levels, Aerojet conducted several tests with the pendulum system at both atmospheric and vacuum conditions. The measured impulse was found to be essentially the same for both conditions. The impulse at each of the four levels was measured as a function of the explosive material weight (W_p), and adjustments to the impulse values used in the missile tests were made because of slight weight variations.

4.2 VKF TESTS

Atmospheric and vacuum tests were made in the dynamic stability laboratory at VKF using the model-balance system that was used in the wind tunnel. The resulting model motion

was recorded on analog tape and then played back through the high-speed scanner and computer to obtain the measured motion (θ_m versus time). Wind-off tests were also conducted in the tank section of the wind tunnel. The action time of the explosive was on the order of 25×10^{-6} sec; therefore, the predicted motion from the analytical model and the measured motion were only compared for 0.4 sec. The amplitude of the initial peak ($t \approx 0.046$ sec) was used to determine the effect of the impulse on the model motion.

The predicted motion from the analytical model was calculated by the following equations. With the model initially at rest (t = 0) and using the assumptions of Section 4.1,

then

$$\text{Impulse} = \text{Change in Angular Momentum}$$

$$r\int_0^{t_1} F\,dt = I(\dot{\theta}_1 - \dot{\theta}_0)$$

$$\dot{\theta}_0 = 0$$

$$(r)(\text{Impulse}) = I\dot{\theta}_1$$

assuming damped free oscillatory motion

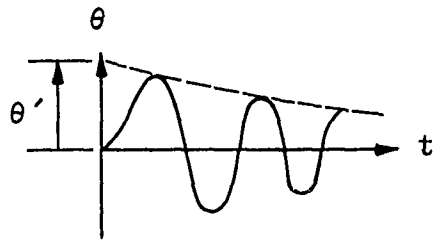

Sketch B

$$\theta = \theta' e^{-\left(\frac{M_{\dot{\theta}}}{2I}\right)t} \sin \omega t \tag{3}$$

$$\dot{\theta} = \theta' \left(-\frac{M_{\dot{\theta}}}{2I}\right) e^{-\left(\frac{M_{\dot{\theta}}}{2I}\right)t} \sin \omega t + \theta' e^{-\left(\frac{M_{\dot{\theta}}}{2I}\right)t} \omega \cos \omega t \tag{4}$$

at $t = t_1$ (t_1 is very small) Eq. (4) becomes

$$\dot{\theta}_1 = \theta' \omega$$

$$(r)(\text{Impulse}) = I\theta'\omega$$

$$\theta' = \frac{(r)(\text{Impulse})}{[-M_\theta I]^{\frac{1}{2}}}$$

where

$$\omega = \left[\frac{-M_\theta}{I}\right]^{\frac{1}{2}}$$

By substituting for θ' in Eq. (3), the predicted motion (θ_p) becomes

$$\theta_p = \left[\frac{(r)(\text{Impulse})}{[-M_\theta I]^{\frac{1}{2}}}\right]\left[e^{-\left(\frac{M_{\dot{\theta}}}{2I}\right)t}\right]\left[\sin \omega t\right] \qquad (5)$$

Equation (5) gives the predicted motion of the analytical model in terms of known quantities and applies for atmospheric, vacuum, and wind-on conditions when the corresponding values are used for M_θ, $M_{\dot{\theta}}$, and ω. The parameters used to calculate the predicted motion were measured during the standard damping tests conducted at the same test conditions as the impulse tests. Therefore, the predicted motion from the analytical model was completely independent of the measured motion.

4.3 PRECISION OF DATA

4.3.1 Tunnel Conditions

Uncertainties (bands which include 95 percent of the calibration data) in the basic tunnel parameters (p_o, T_o, and M_∞) were estimated from repeat calibrations of the instrumentation and from repeatability and uniformity of the test section flow during tunnel calibrations. These uncertainties were used to estimate uncertainties in other free-stream properties using

a Taylor series method of error propagation (Ref. 4). The estimated uncertainties for the two Reynolds numbers of this test are as follows:

Uncertainty, percent					
M_∞	p_o	T_o	q_∞	V_∞	Re_ℓ
±0.7	±0.2	±0.5	±1.8	±0.4	±1.3

4.3.2 Impulse Data

The repeatability of the impulse was estimated by Aerojet to be within ±5 percent. The wind-off tests show that the predicted motion is within 5 percent of the measured motion for 80 percent of the test firings. Therefore, using the wind-off tests as a measure of the uncertainty, the estimated uncertainty in the predicted motion (analytical model) is considered to be ±5 percent. The estimated uncertainty in angle of attack and amplitude of oscillation is ±0.1 deg and ±0.5 percent, respectively.

5.0 RESULTS AND DISCUSSION

The results of the VKF laboratory impulse tests are shown in Fig. 9. The predicted and measured motion as a function of time are presented for eight impulse tests at atmospheric and vacuum conditions. Since there is no aerodynamic flow field for the impulse explosion to interact with, then these results indicate how well the analytical model (predicted motion) predicts the model motion produced by the impulse. As can be seen from the plotted results, the analytical model is good. The results of the impulse tests in the Tunnel A tank are shown in Fig. 10. Of the ten wind-off impulse tests (eight in the laboratory and two in the Tunnel A tank), eight of these show the predicted motion to be within 3.9 percent of the measured motion which is within the system's estimated uncertainty of ±5 percent. The reason for the larger differences (6.6 and 7.4 percent) obtained in the other two tests is unknown. A summary of the wind-off impulse tests is presented in Table 2.

Figure 11 shows an outline of the schlieren photographs for the purpose of identifying apparatus and shocks shown on the photographs. VKF laboratory tests showed that the plexiglass particles from the cover would damage a steel plate approximately 20 in. from the model nose (same distance as

tunnel nozzle plate). In order to protect the tunnel nozzle plate from the plexiglass particles, a rubber mat was positioned on the plate such that the leading edge shock would miss the model tail. These shocks are clearly evident in the schlieren photographs and are identified in Fig. 11. The AFATL program called for the test to be conducted at $x_p/\ell = 0.329$ which located the model tail section far aft of the strut-support sting junction (Fig. 7). The junction of the strut and sting produced shocks (Fig. 11) which impinged on the model tail. Since these shocks from the sting-strut junction were present for both the pitch-damping tests and the impulse tests, it is felt that the evaluation of the impulse effect on the model motion is still valid. However, for this reason damping coefficients are not presented in this report.

Color schlieren photographs of the impulse tests are presented in Figs. 12 and 13. High-speed (7,500 frames/sec), 16-mm color schlieren motion-pictures were taken of the impulse tests, and prints (Figs. 12 and 13) were then made of the individual frames of the motion-picture film. In Fig. 12 (forward portion of the model), the first frame of the explosion is defined as t = 0 and succeeding frames are then time oriented for the purpose of understanding the rate of movement of the impulse mass along the model. In Fig. 13 (aft portion of the model), each frame is time oriented with respect to the first frame of the explosion (t = 0). It should be noted that $\alpha = 0.94$ deg for Fig. 12 and 2.02 deg for Fig. 13. Figures 12 and 13 show that the impulse mass produced large effects on the model flow field and created a blast shock wave as would be expected.

The plotted results of the ten impulse tests in Tunnel A are shown in Figs. 14, 15, and 16. The predicted and measured model motion are presented in Fig. 14 for forward impulse firings and in Fig. 15 for aft impulse firings, both at $Re_\ell = 12.2 \times 10^6$. Figure 16 shows data for two aft impulse firings at $Re_\ell = 23.1 \times 10^6$. The data show that the measured motion agrees well with the predicted motion. The measured motion (initial peak) was 3 to 7.6 percent larger than the predicted motion which was about the same difference as was found in the wind-off data (laboratory and Tunnel A tank). Thus, these data indicate that with the short time of the flow field disturbance (0.003 to 0.004 sec), the blast wave induced pressures were not large enough to influence the model motion. A summary of the air-on impulse tests is presented in Table 3.

6.0 SUMMARY OF RESULTS

Wind tunnel tests were conducted to determine if the interaction of the impulse explosion with the supersonic airflow caused an effect on the model motion. The free oscillation cross flexure technique was utilized to measure the motion produced by the impulse and also the model aerodynamic stiffness and damping. Tests were conducted at Mach number 3, and data were obtained at Reynolds numbers, based on model length, of 12.2×10^6 and 23.1×10^6. A summary of results based on the data presented in this report is given below:

1. The analytical model predicted the wind-off model motion due to impulse well; therefore for wind-on conditions, it provided a good means for evaluating the effect of the perturbed flow field on the model motion.

2. Although schlieren photographs indicated that the model flow field was significantly disturbed by the explosion, the perturbed flow field, lasting only for 0.003 to 0.004 sec, did not produce any significant effects on the model motion.

REFERENCES

1. Strike, William, T., Jr. "Analyses of the Aerodynamic Disturbances Generated on a Flat Plate Containing Lateral Jet Nozzles Located in a Hypersonic Stream." AEDC-TR-67-158 (AD826485), January 1968.

2. Uselton, Bob L. and Uselton, James C. "Test Mechanism for Measuring Pitch-Damping Derivatives of Missile Configurations at High Angles of Attack." AEDC-TR-75-43 (ADA009865), May 1975.

3. Schueler, C. J., Ward, L. K., and Hodapp, A. E., Jr. "Techniques for Measurement of Dynamic Stability Derivatives in Ground Test Facilities." AGARDograph 121 (AD669227), October 1967.

4. Beers, Yardley. Introduction to the Theory of Error. Addison-Wesley Publishing Co., Inc., Reading, Massachusetts, 1957, pp. 26-36.

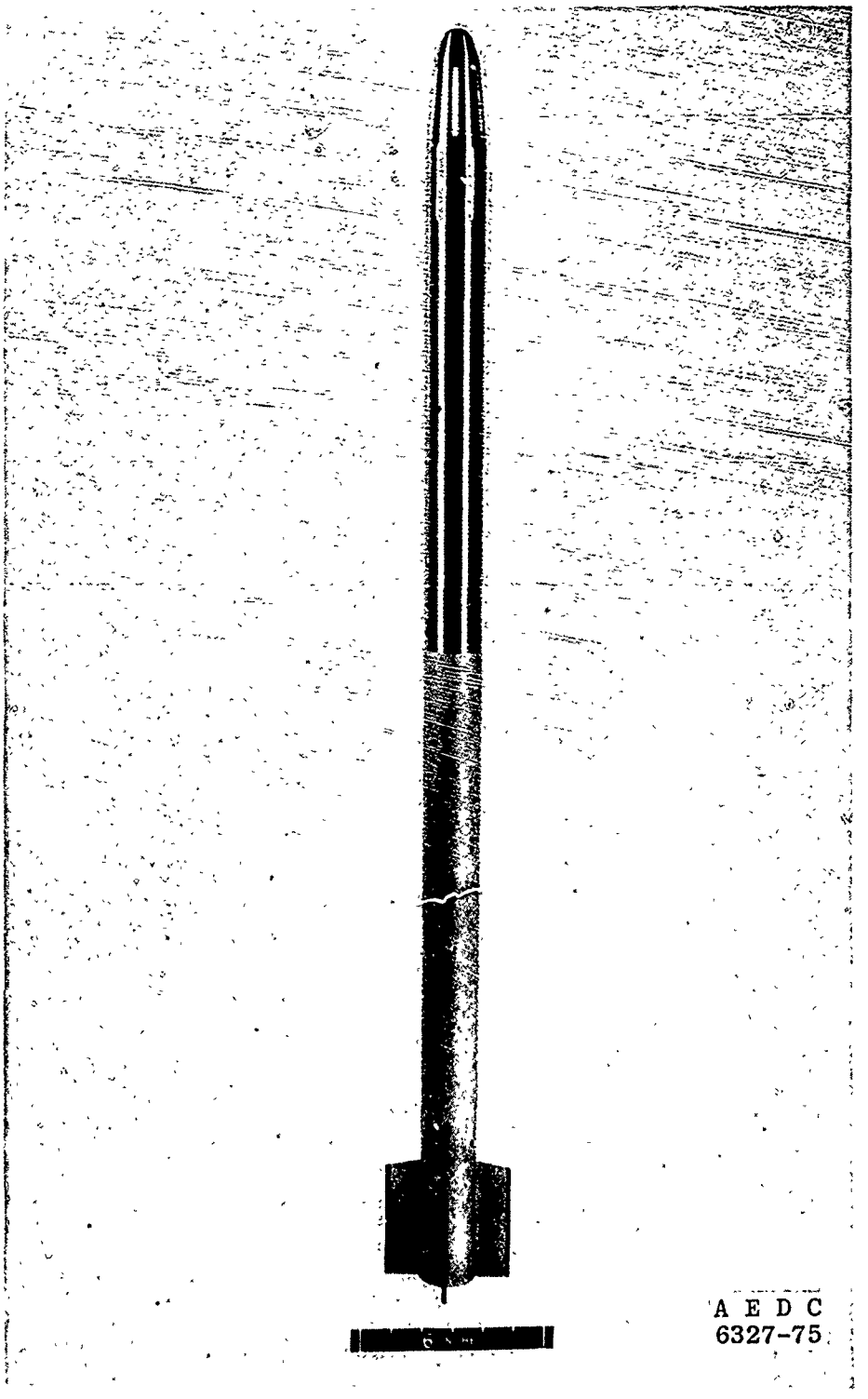

Figure 1. Photograph of the model.

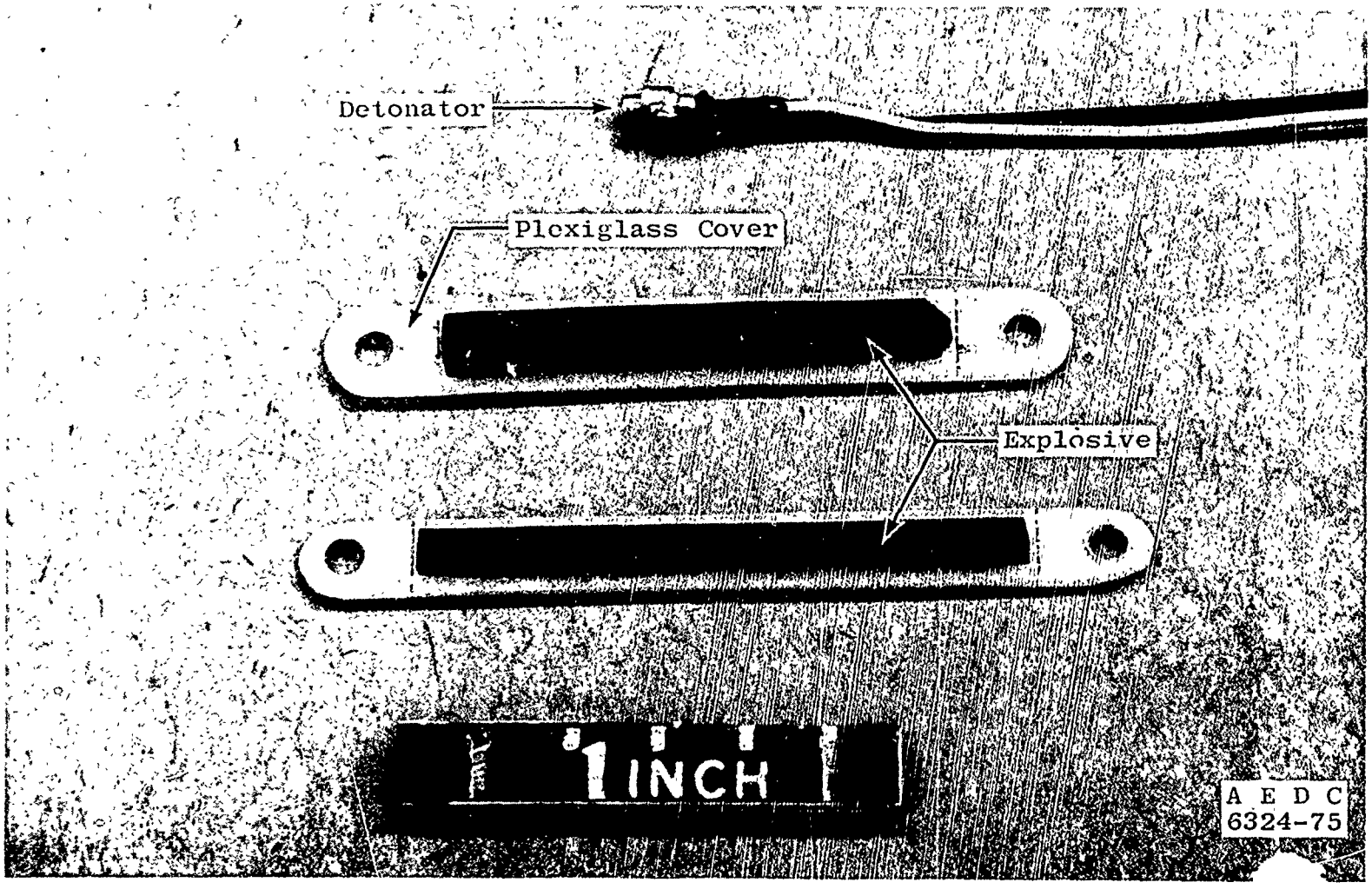

Figure 2. Photograph of the detonator, explosive, and plexiglass cover.

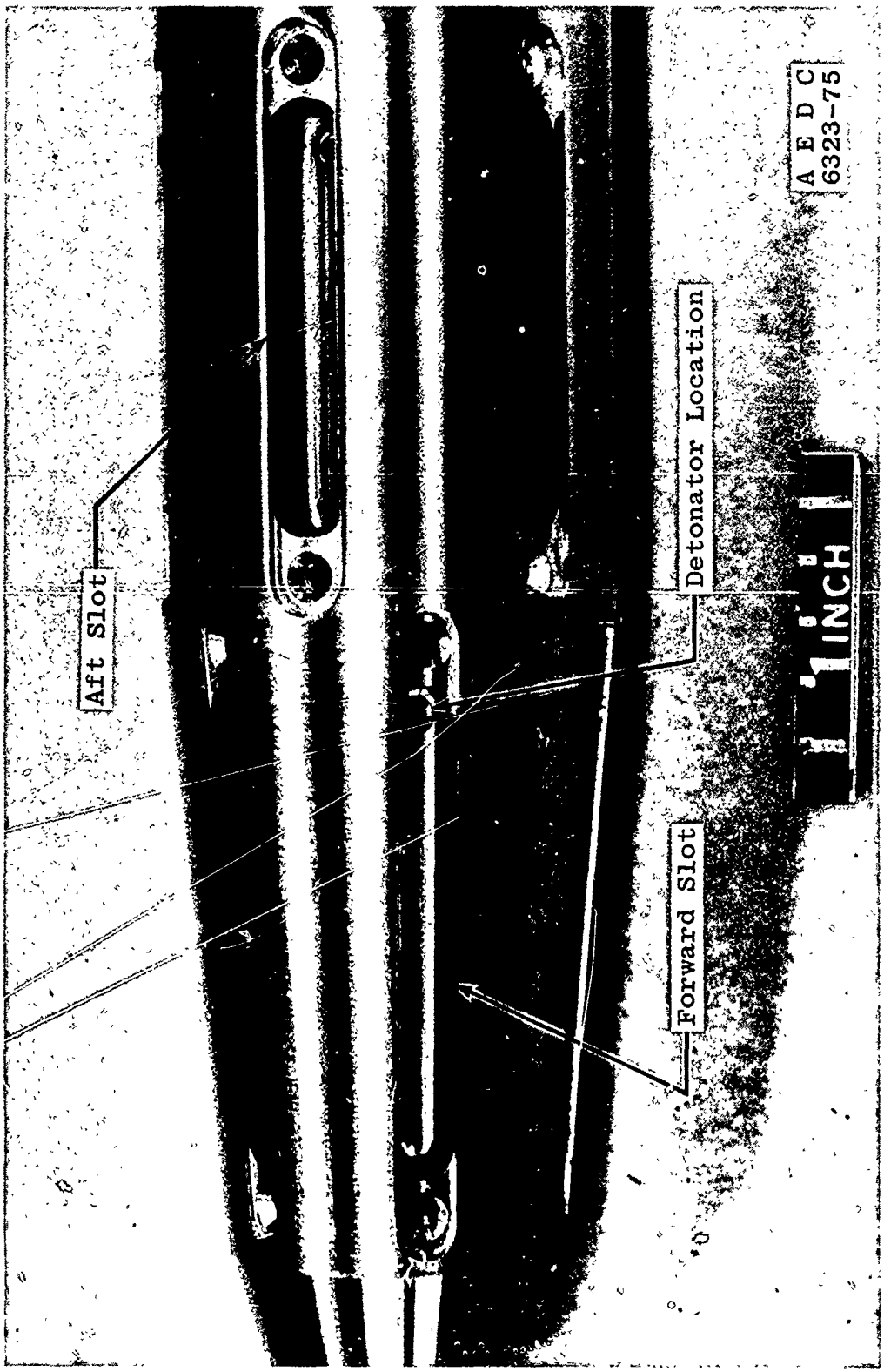

Figure 3. Photograph of the model nose slots.

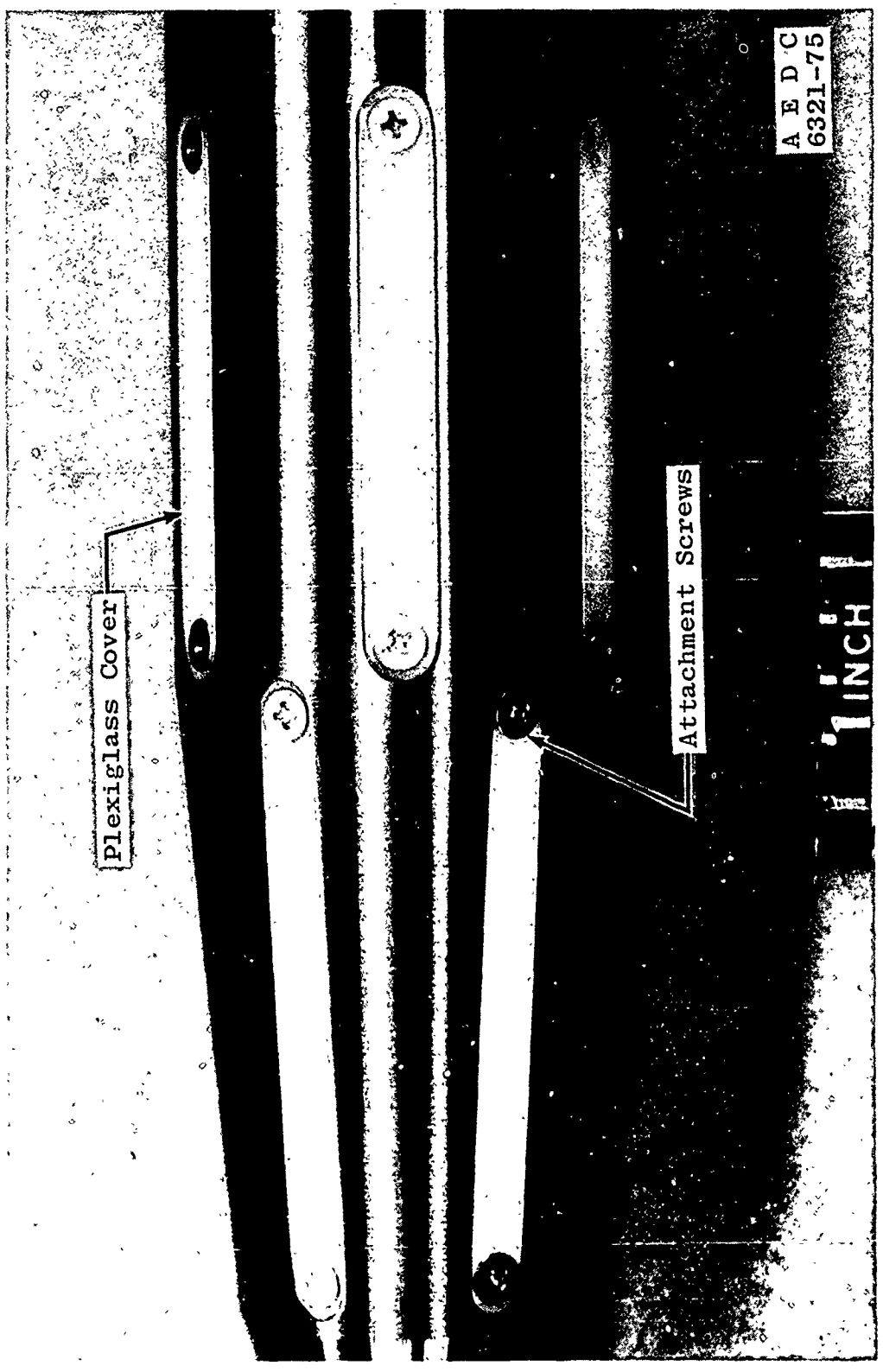

Figure 4. Photograph of the model nose with plexiglass covers installed.

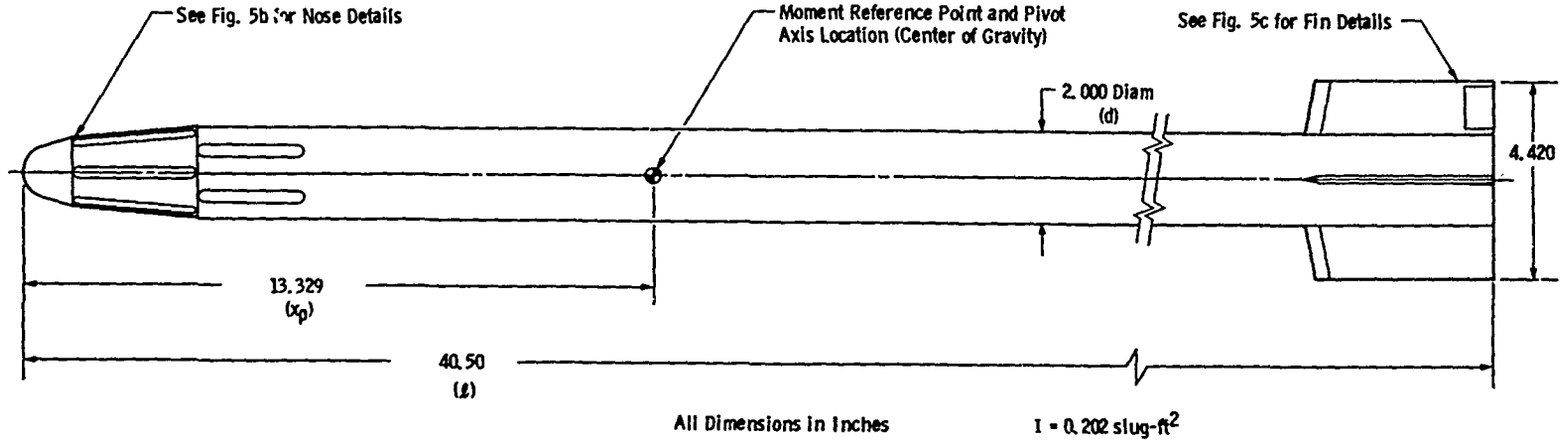

a. Overall model geometry

Figure 5. Model details.

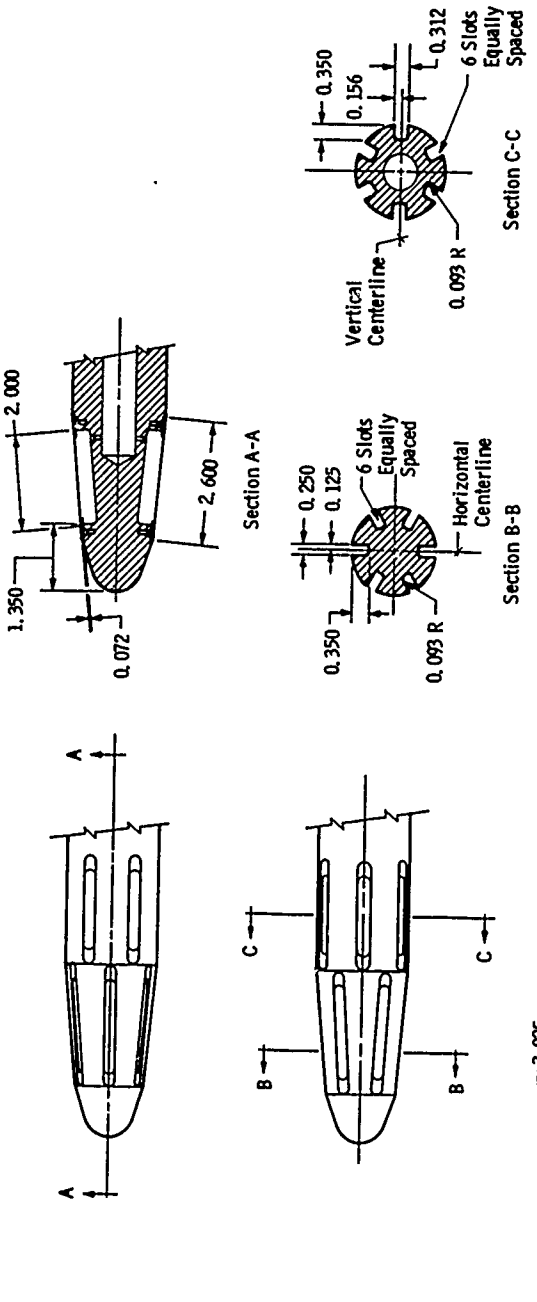

b. Nose details
Figure 5. Continued.

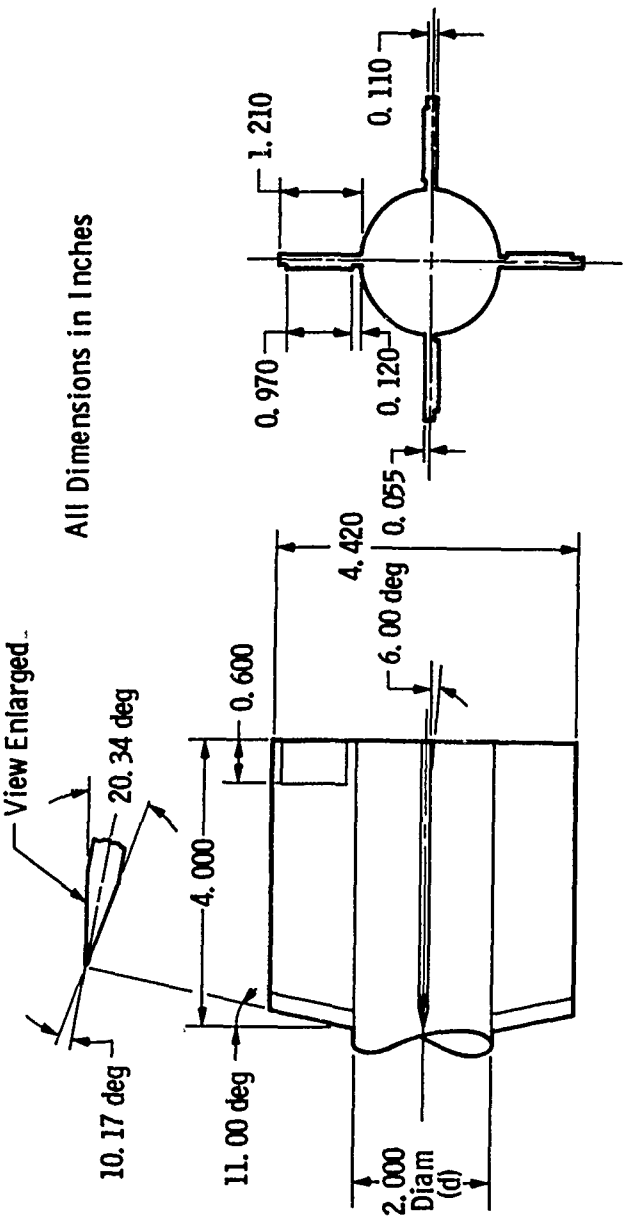

c. Fin details
Figure 5. Concluded.

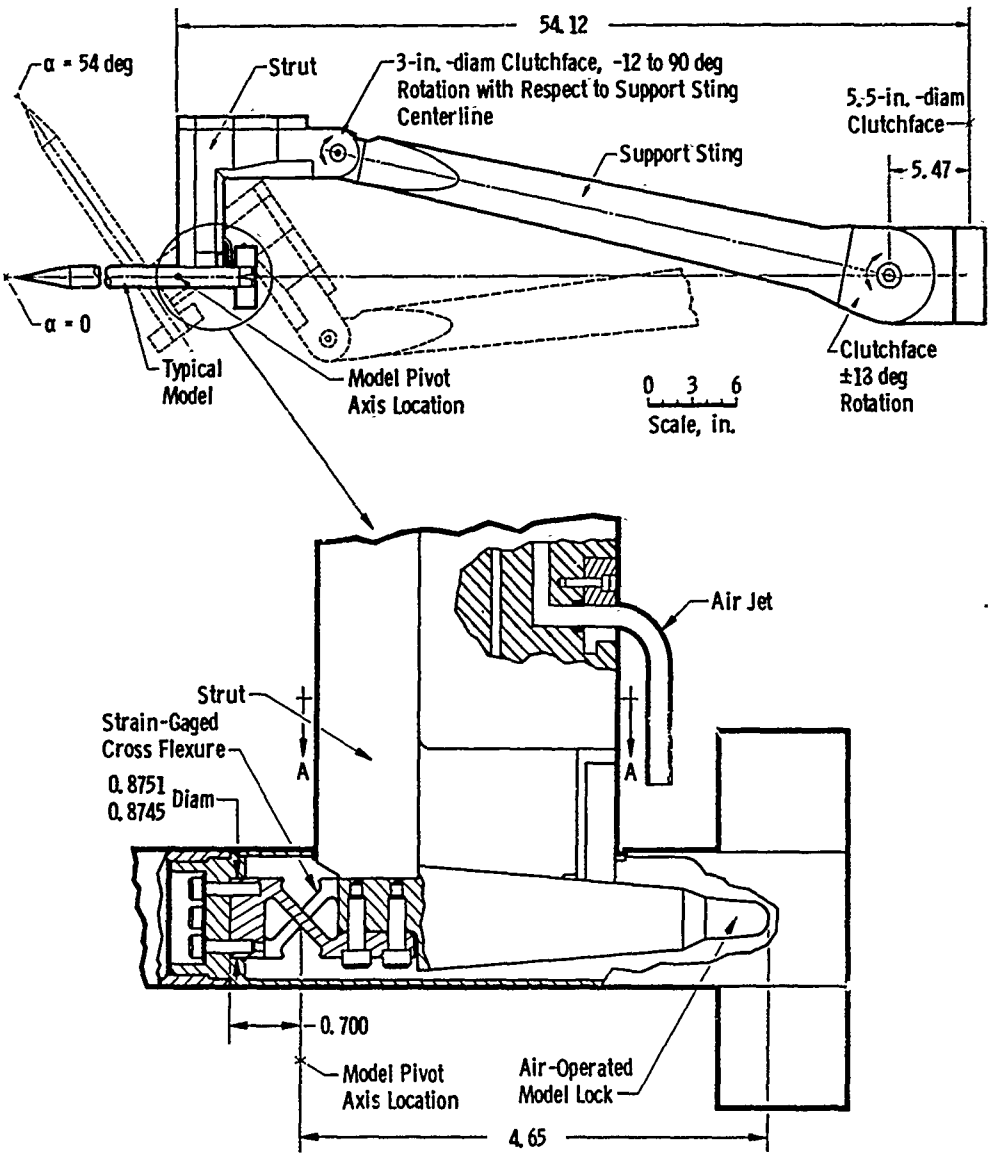

All Dimensions in Inches

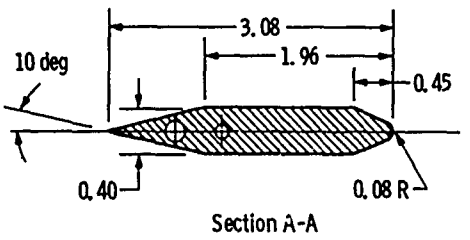

Figure 6. VKF 2.G high-alpha pitch-damping test mechanism.

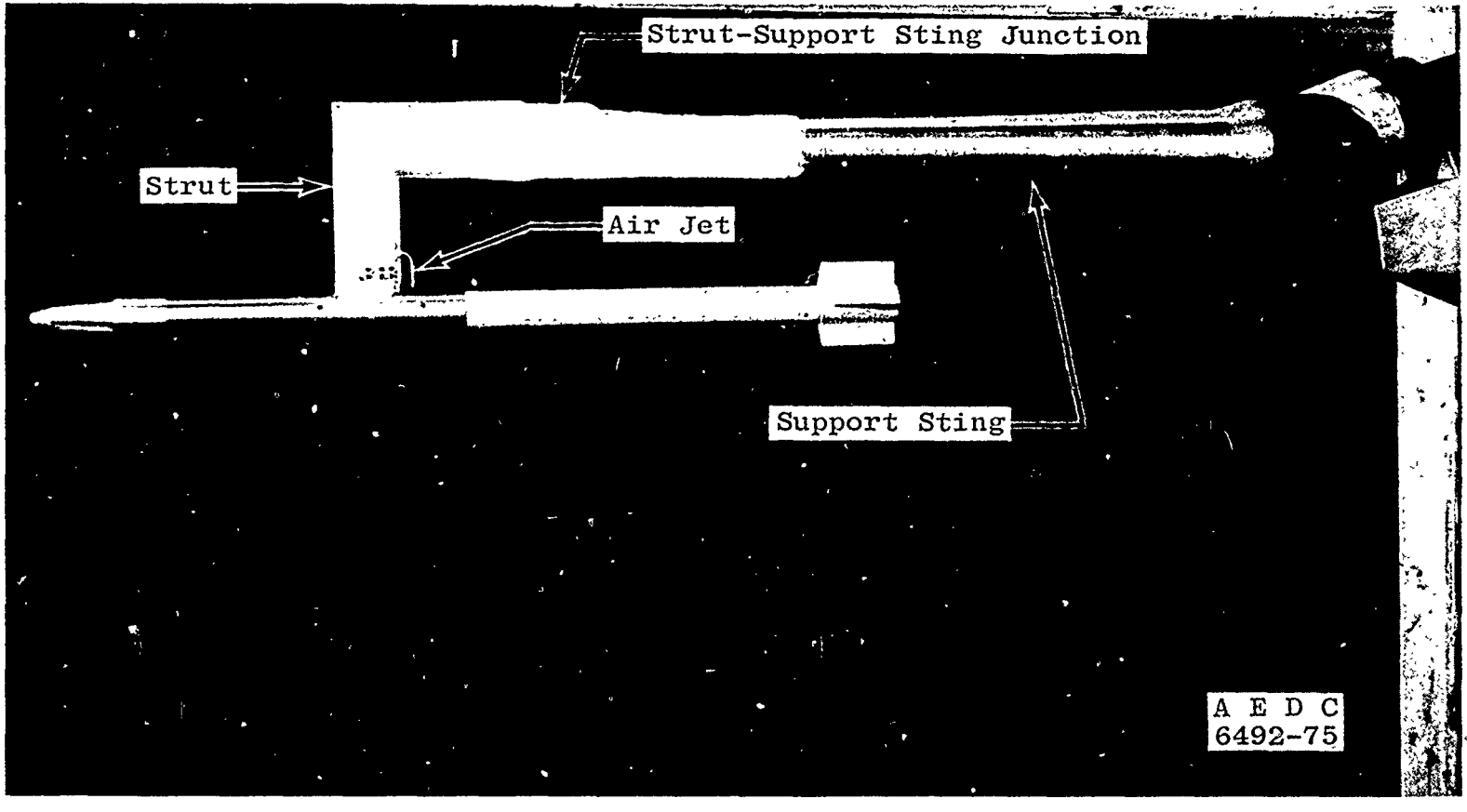

Figure 7. Photograph of the model installation.

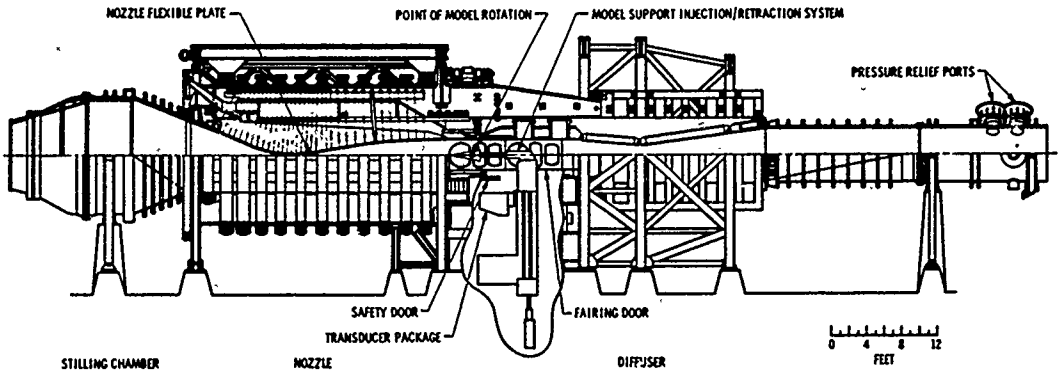

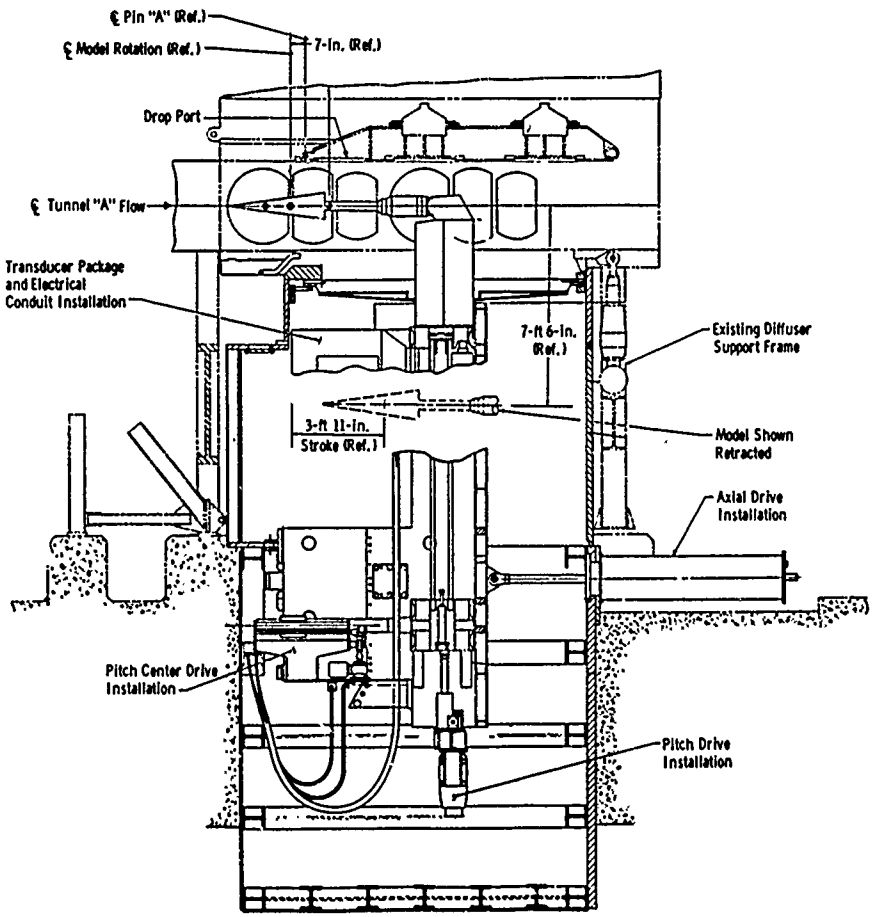

Figure 8. Tunnel A details.

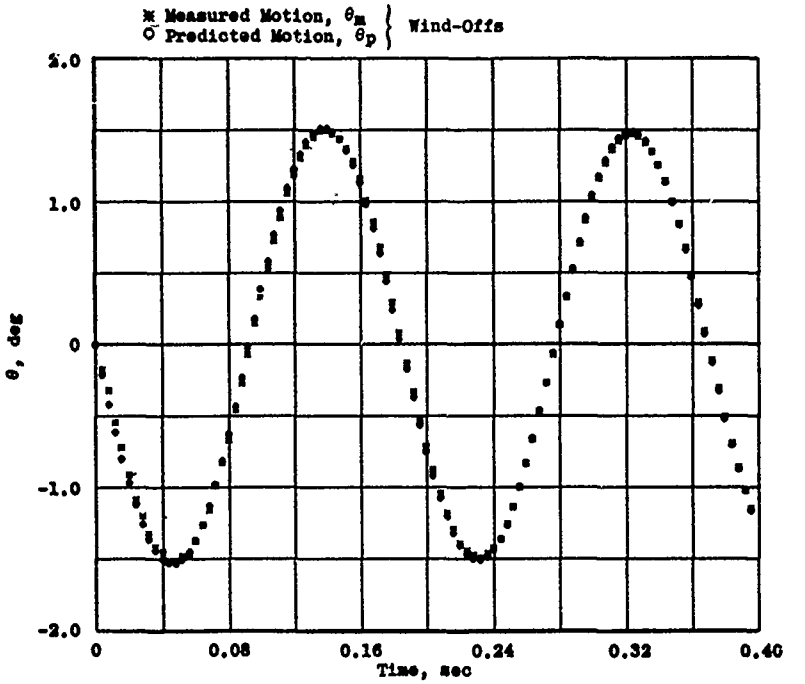

a. Test 1, $\overline{\theta}_m/\overline{\theta}_p$ = 1.005, forward impulse = -0.201 lb-sec, p = 14.2 psia

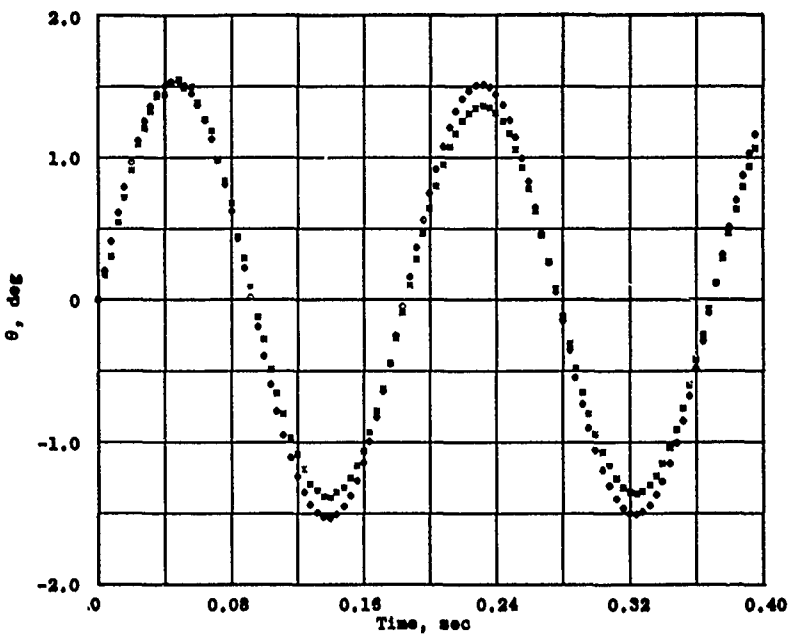

b. Test 2, $\overline{\theta}_m/\overline{\theta}_p$ = 1.014, forward impulse = 0.202 lb-sec, p = 0.2 psia

Figure 9. Comparison of predicted and measured motion from impulse tests in the VKF laboratory.

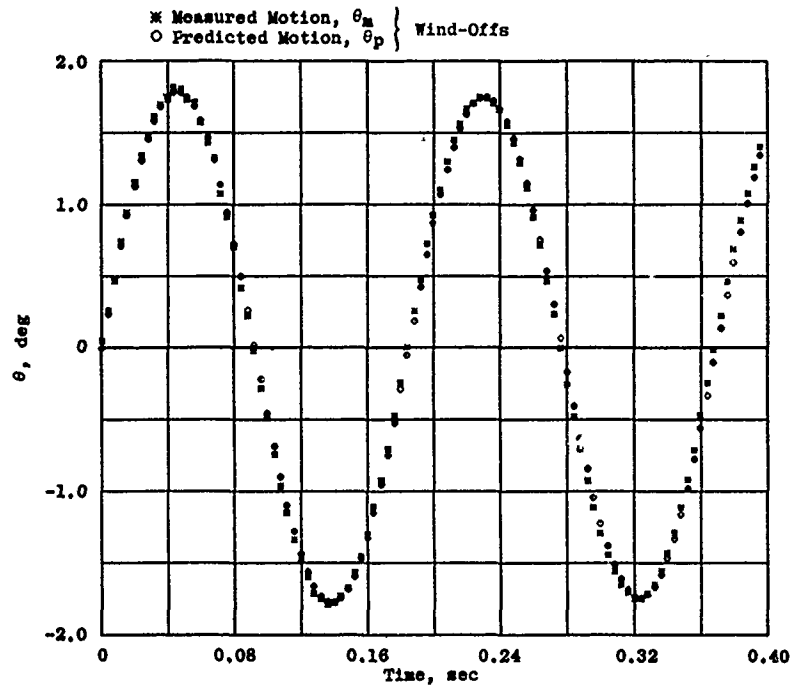

c. Test 3, $\overline{\theta}_m/\overline{\theta}_p$ = 1.030, forward impulse = 0.234 lb-sec, p = 14.2 psia

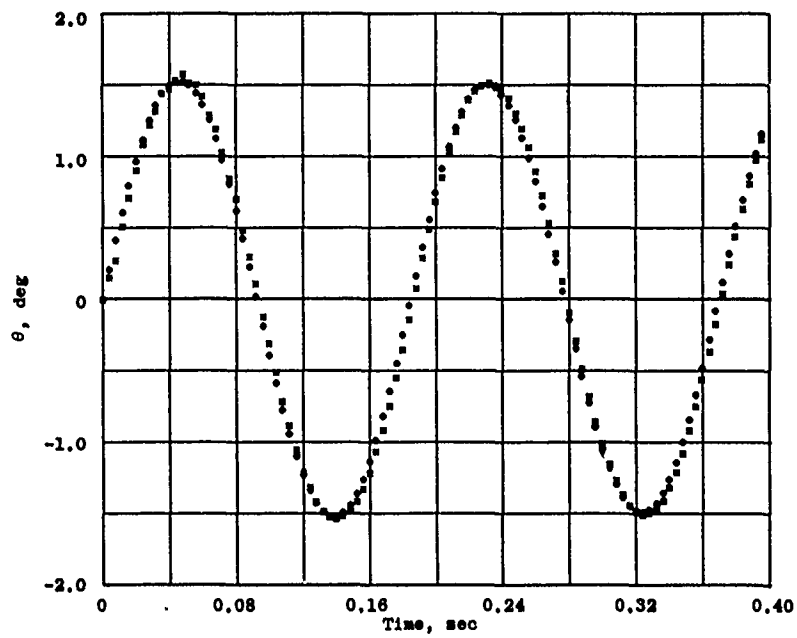

d. Test 4, $\overline{\theta}_m/\overline{\theta}_p$ = 1.029, aft impulse = 0.259 lb-sec, p = 14.2 psia

Figure 9. Continued.

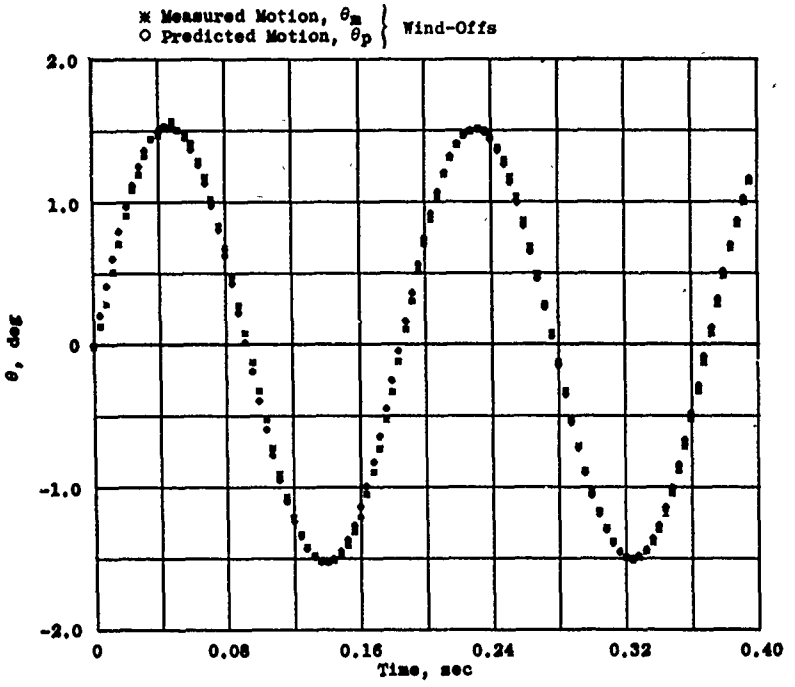

e. Test 5, $\overline{\theta}_m/\overline{\theta}_p$ = 1.023, aft impulse = 0.260 lb-sec, p = 14.2 psia

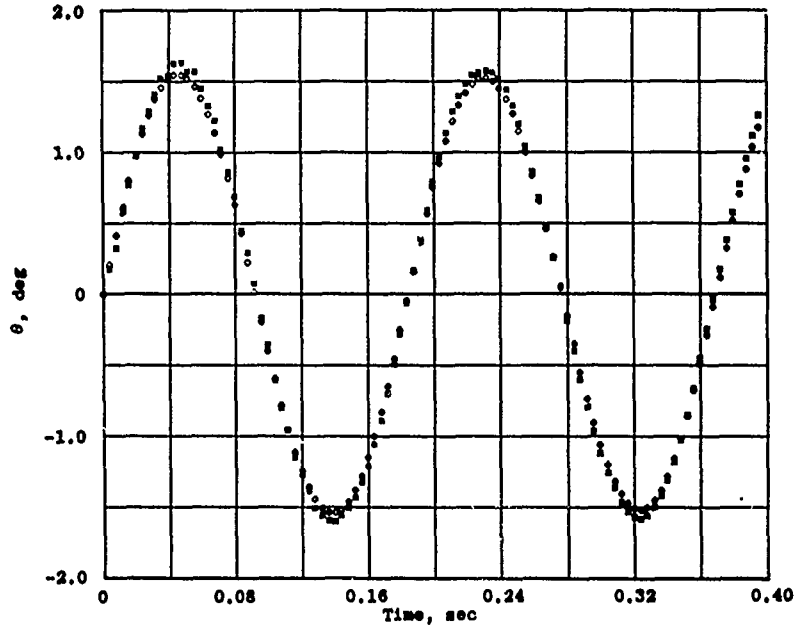

f. Test 6, $\overline{\theta}_m/\overline{\theta}_p$ = 1.066, aft impulse = 0.262 lb-sec, p = 0.2 psia

Figure 9. Continued.

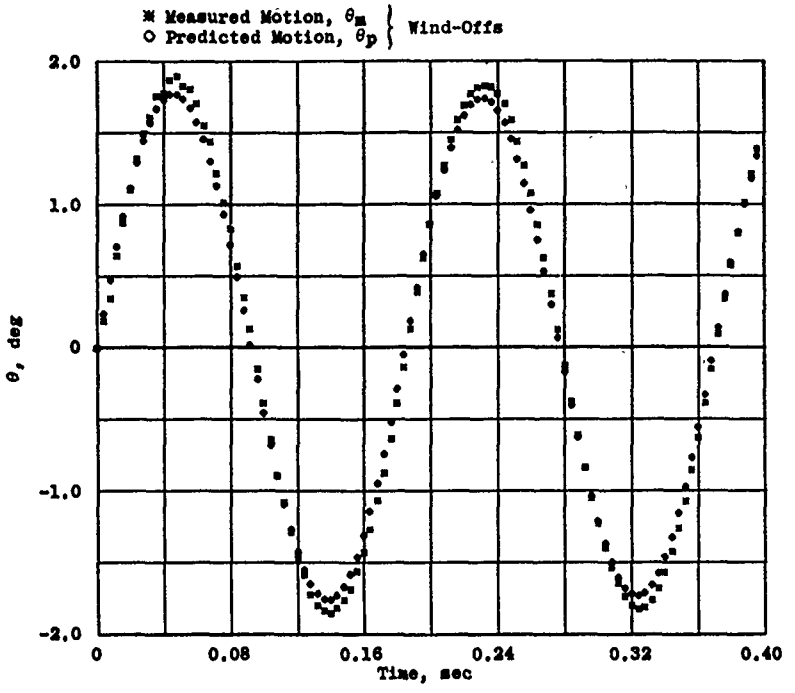

g. Test 7, $\overline{\theta}_m/\overline{\theta}_p$ = 1.074, aft impulse = 0.300 lb-sec, p = 0.2 psia

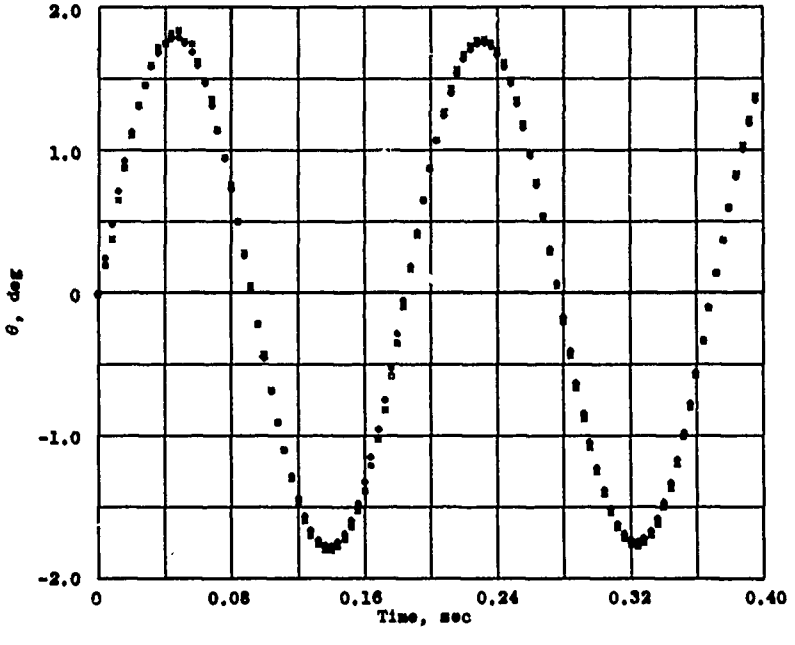

h. Test 8, $\overline{\theta}_m/\overline{\theta}_p$ = 1.034, aft impulse = 0.303 lb-sec, p = 14.2 psia

Figure 9. Concluded.

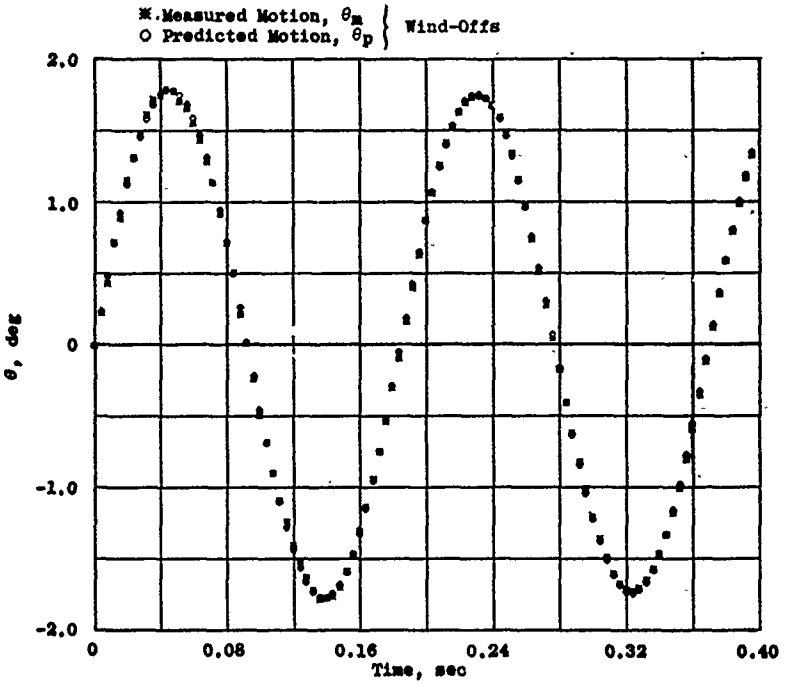

a. Test 9, $\overline{\theta}_m/\overline{\theta}_p$ = 1.020, impulse = 0.234 lb-sec

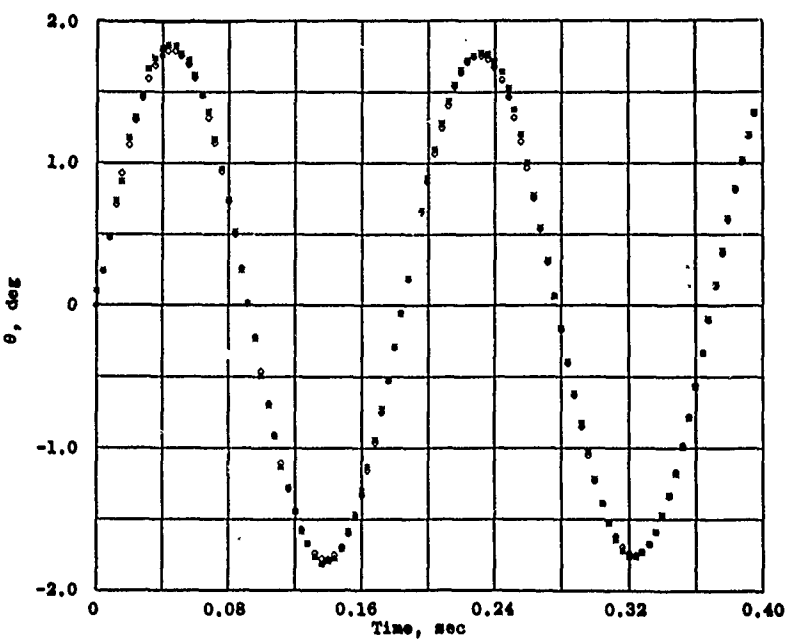

b. Test 10, $\overline{\theta}_m/\overline{\theta}_p$ = 1.039, impulse = 0.236 lb-sec

Figure 10. Comparison of predicted and measured motion from wind-off impulse tests in Tunnel A tank, forward impulse, p = 14.2 psia.

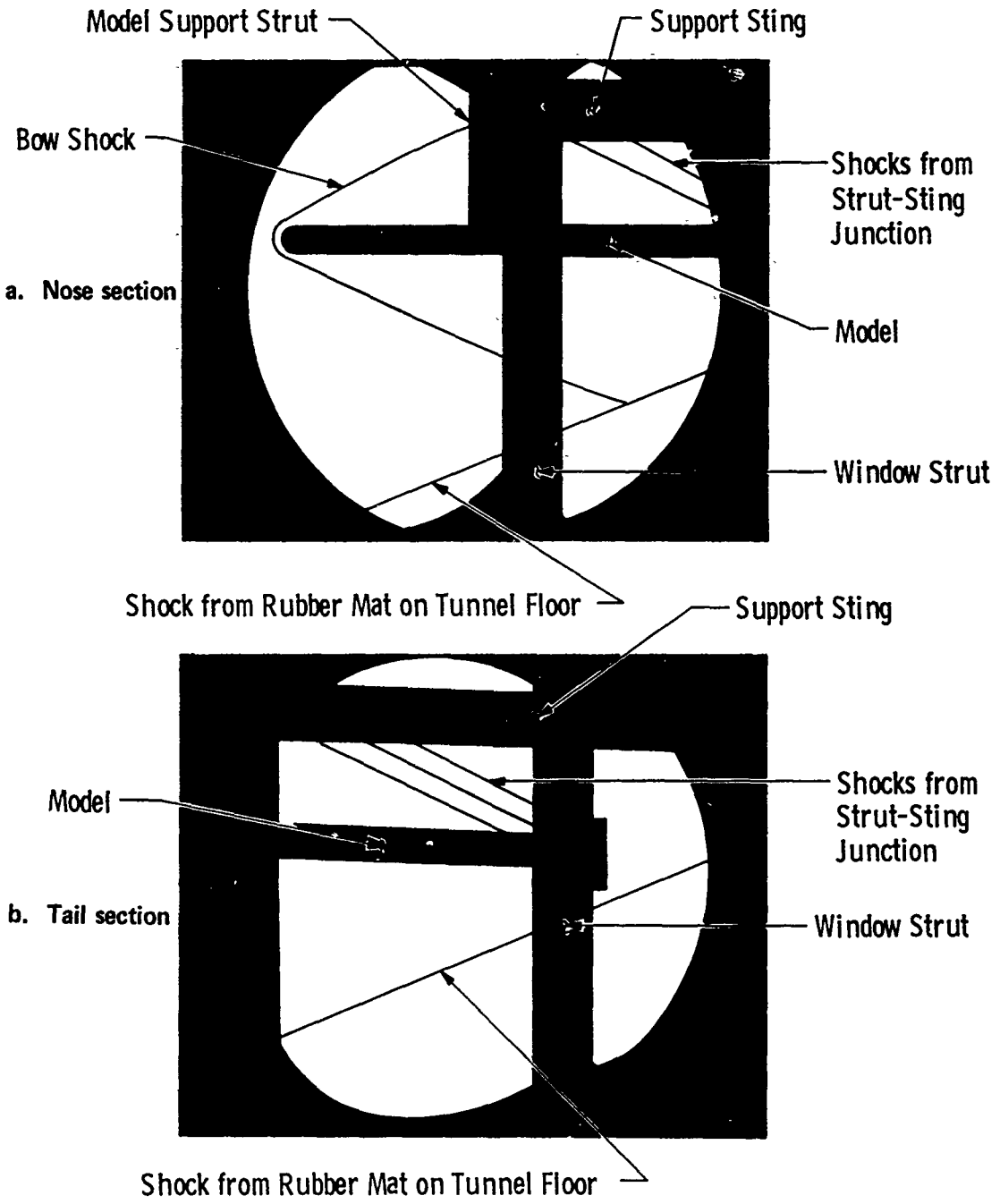

Figure 11. Identification of schlieren photographs.

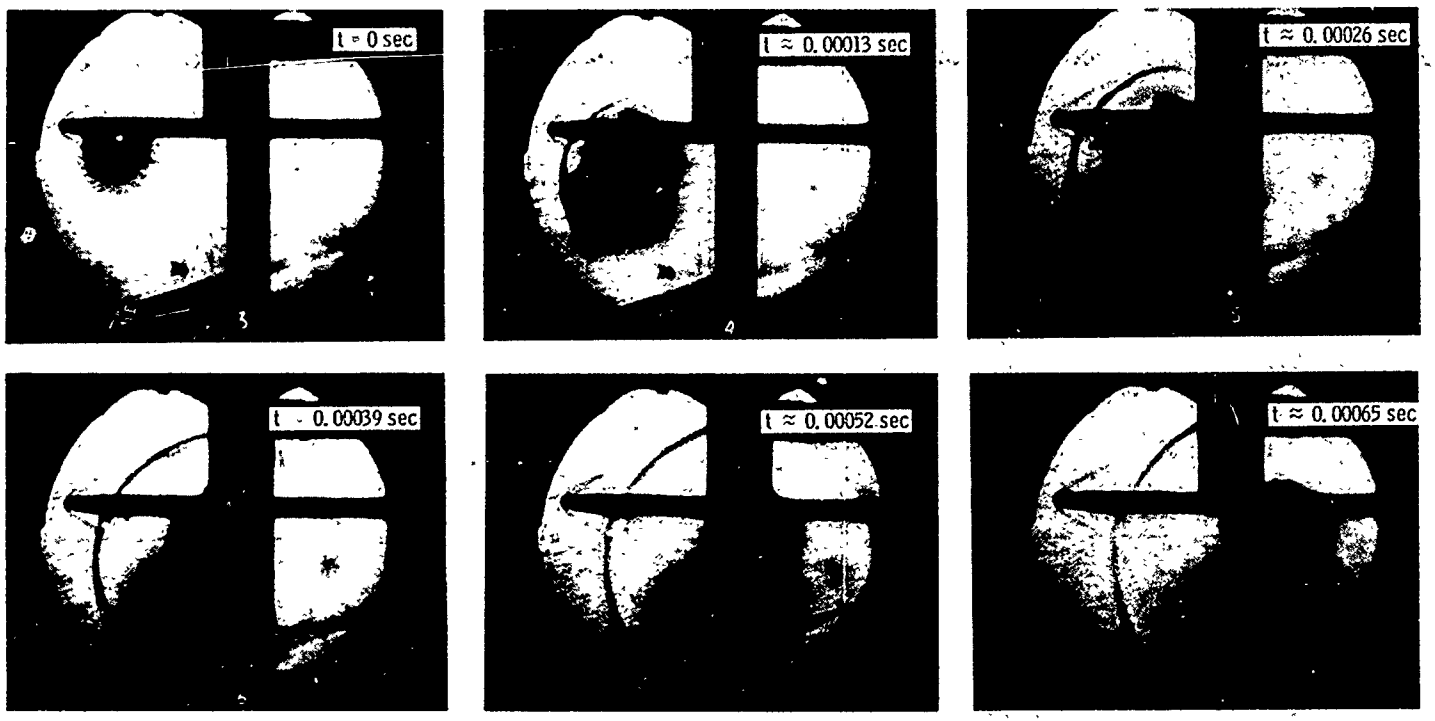

Figure 12. Schlieren photographs showing the effect of the impulse on the flow field about the forward portion of the model—$M_\infty = 3$, $\alpha = 0.94$ deg, $Re_\ell = 12.2 \times 10^6$, Test 13.

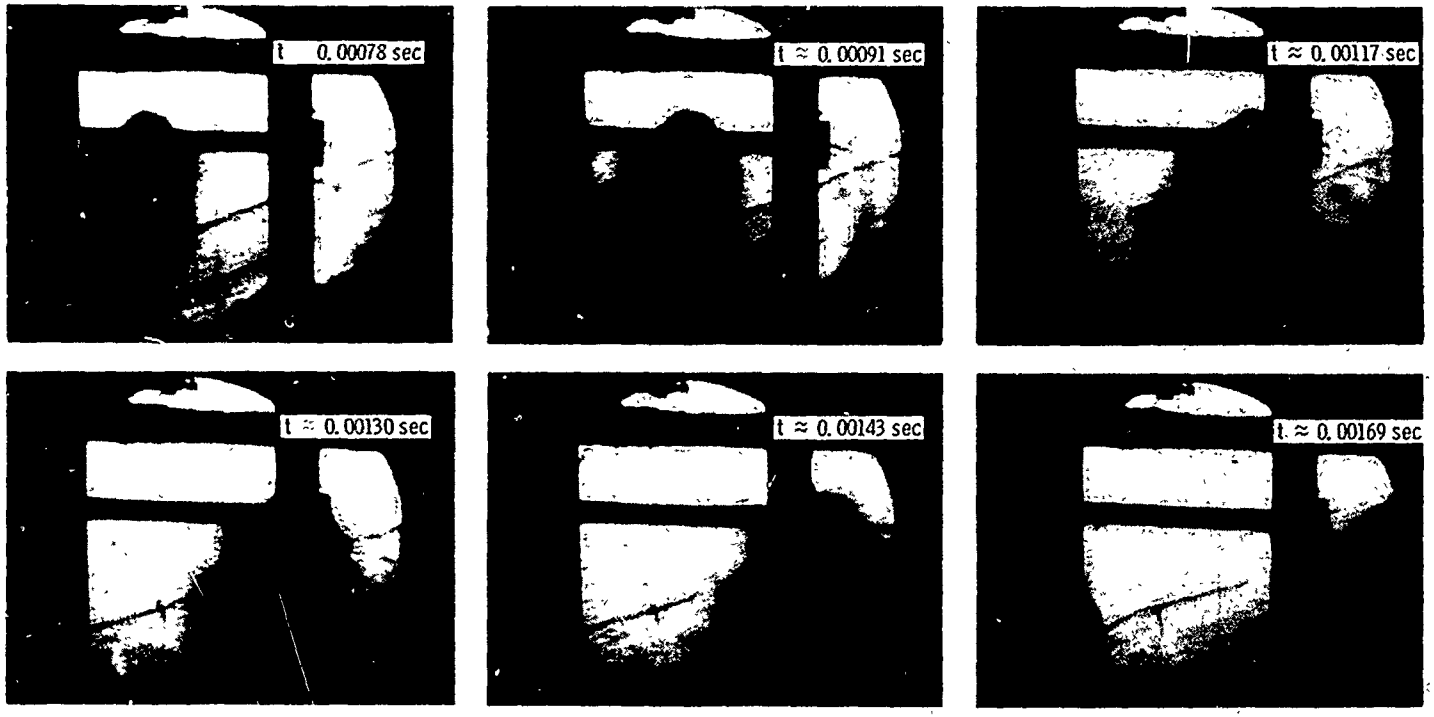

Figure 13. Schlieren photographs showing the effect of the impulse on the flow field about the aft portion of the model--M_∞ = 3, α = 2.02 deg, Re_ℓ = 12.2 x 10^6, Test 15.

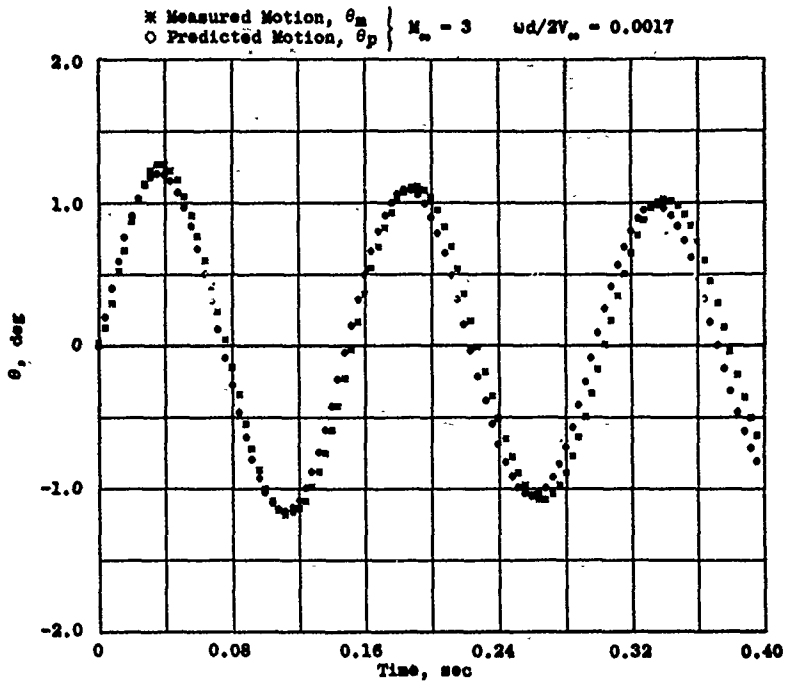

a. Test 11, $\overline{\theta}_m/\overline{\theta}_p = 1.059$, $\alpha = 1.14$ deg, impulse = 0.201 lb-sec

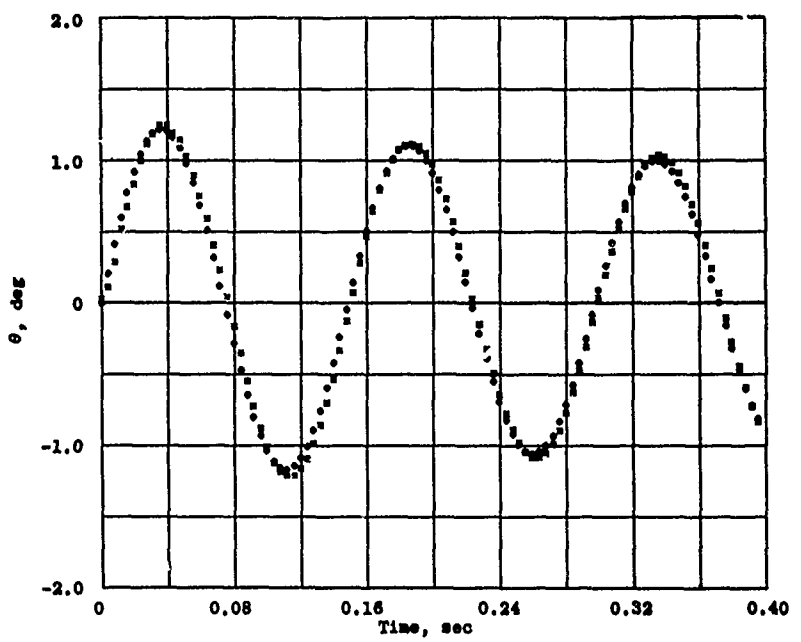

b. Test 12, $\overline{\theta}_m/\overline{\theta}_p = 1.030$, $\alpha = 0.96$ deg, impulse = 0.203 lb-sec

Figure 14. Comparison of predicted and measured motion from impulse tests in Tunnel A, forward impulse, $Re_\ell = 12.2 \times 10^6$.

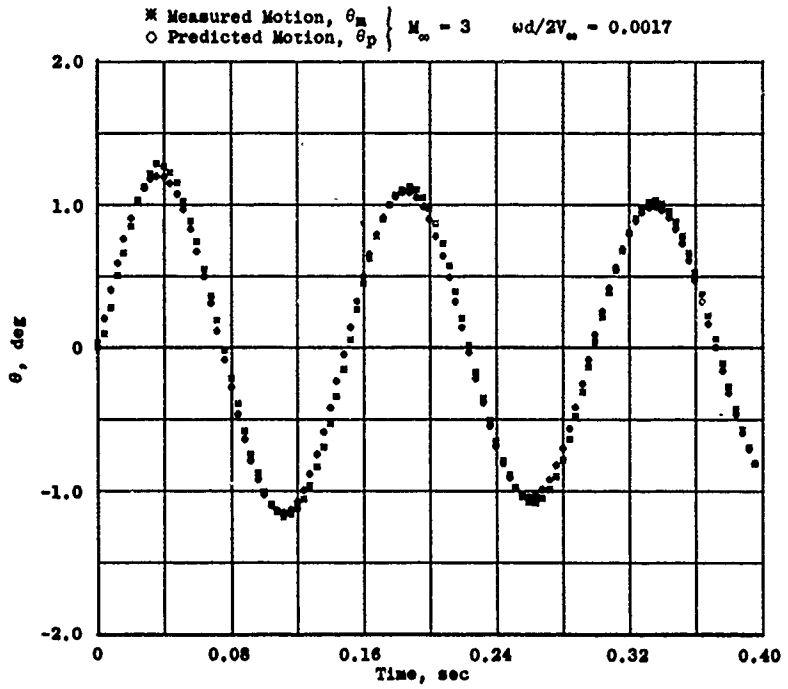

a. Test 13, $\overline{\theta}_m/\overline{\theta}_p$ = 1.073, a = 0.94 deg, impulse = 0.258 lb-sec

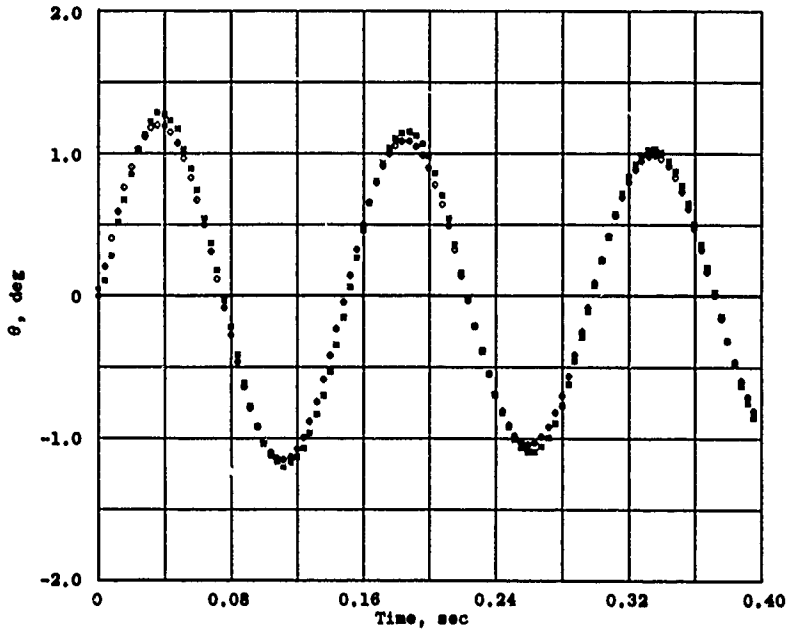

b. Test 14, $\overline{\theta}_m/\overline{\theta}_p$ = 1.069, a = 0.98 deg, impulse = 0.258 lb-sec

Figure 15. Comparison of predicted and measured motion from impulse tests in Tunnel A, aft impulse, $Re_\ell = 12.2 \times 10^6$.

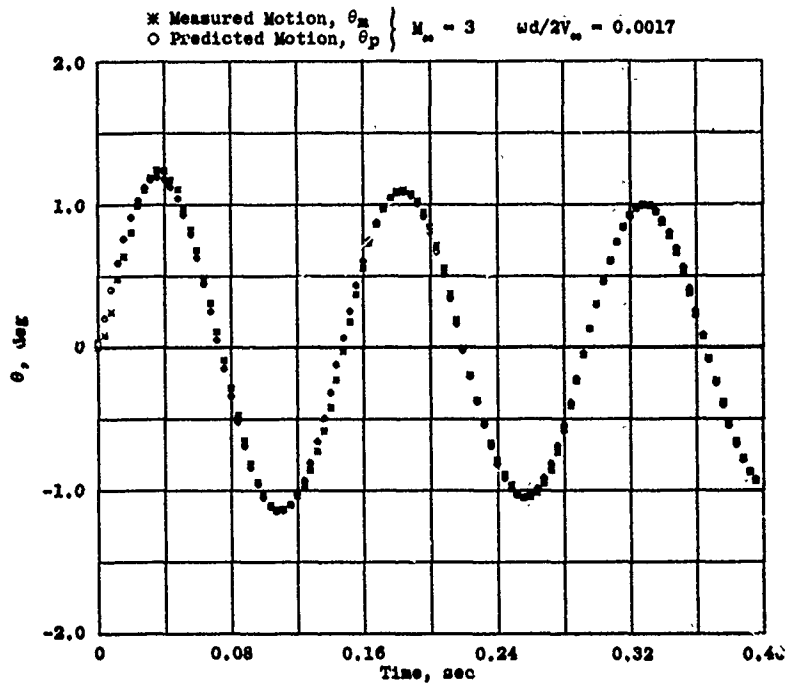

c. Test 15, $\overline{\theta}_m/\overline{\theta}_p$ = 1.044, α = 2.02 deg, impulse = 0.259 lb-sec

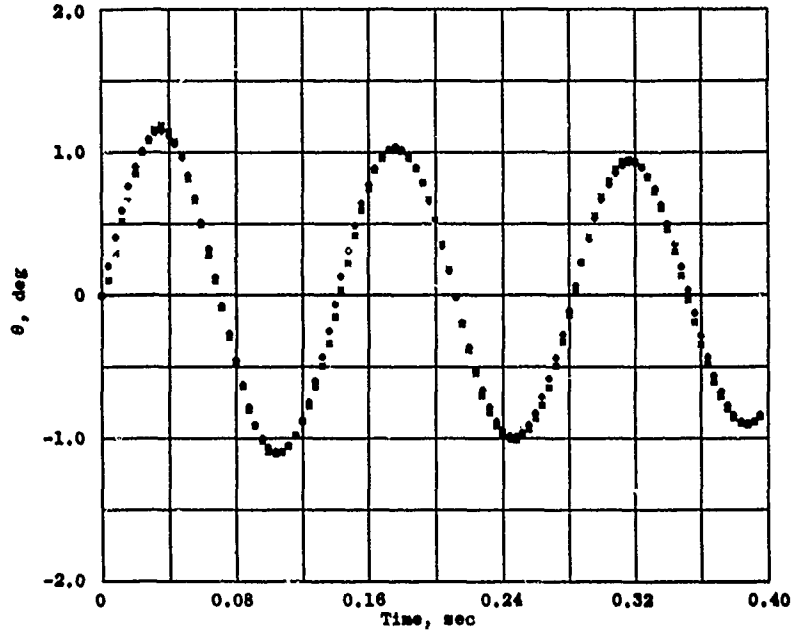

d. Test 16, $\overline{\theta}_m/\overline{\theta}_p$ = 1.036, α = 3.11 deg, impulse = 0.260 lb-sec

Figure 15. Continued.

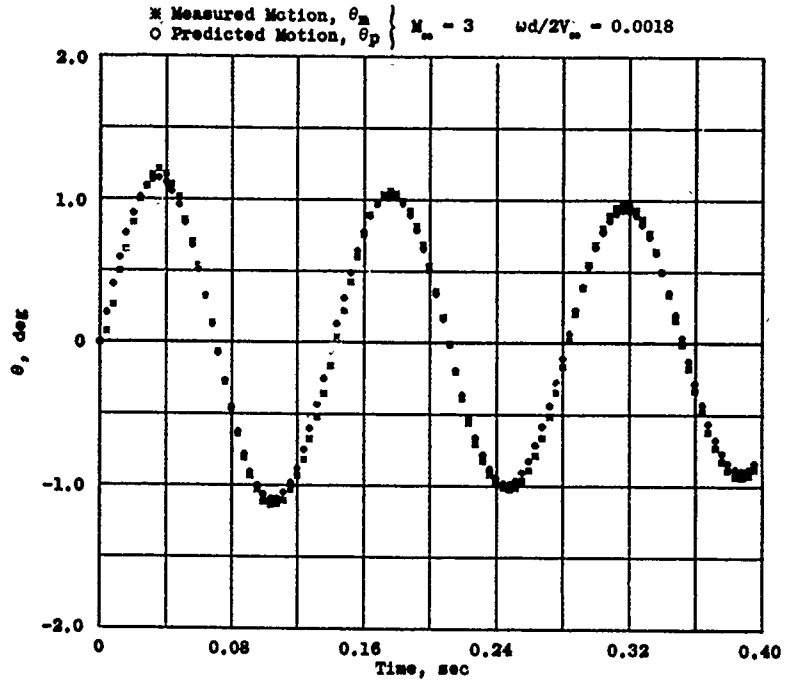

e. Test 17, $\bar{\theta}_m/\bar{\theta}_p$ = 1.053, α = 3.08 deg, impulse = 0.260 lb-sec

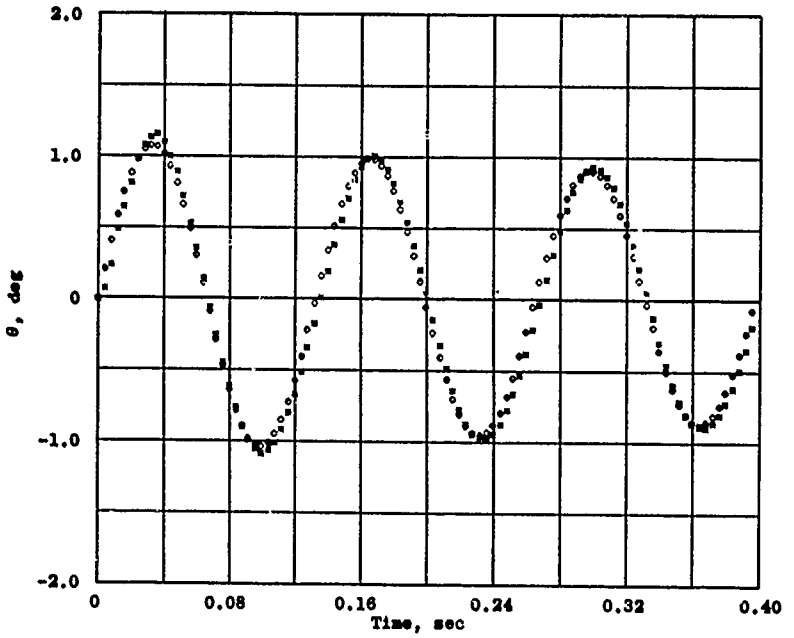

f. Test 18, $\bar{\theta}_m/\bar{\theta}_p$ = 1.076, α = 4.42 deg, impulse = 0.259 lb-sec

Figure 15. Concluded.

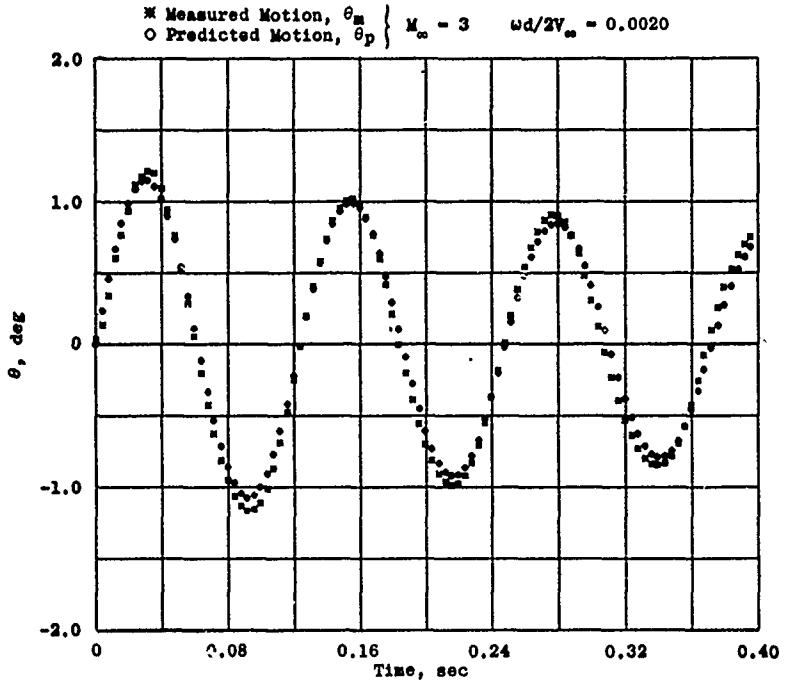

a. Test 19, $\overline{\theta}_m/\overline{\theta}_p$ = 1.053, α = 2.64 deg, impulse = 0.301 lb-sec

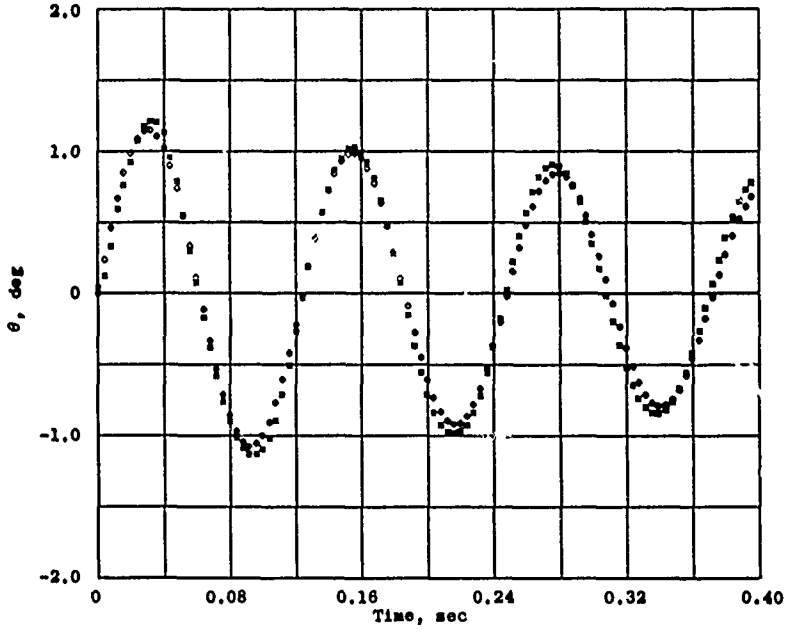

b. Test 20, $\overline{\theta}_m/\overline{\theta}_p$ = 1.063, α = 2.64 deg, impulse = 0.301 lb-sec

Figure 16. Comparison of predicted and measured motion from impulse tests in Tunnel A, aft impulse, $Re_\ell = 23.1 \times 10^6$.

Table 1. Tunnel Conditions

M_∞	$Re_\ell \times 10^{-6}$	p_o, psia	T_o, °R	q_∞, psia	V_∞, ft/sec
3.01	12.2	24.80	563	4.22	2088
3.01	23.1	47.57	567	8.09	2095

Table 2. Summary of VKF Laboratory and Tunnel A Tank Results

Test	Location	p, psia	W_p, gram	Impulse, lb-sec	$\bar{\theta}_p$, deg	$\bar{\theta}_m$, deg	$\frac{\bar{\theta}_m}{\bar{\theta}_p}$
1	lab	14.2	0.317	-0.201	-1.532	-1.540	1.005
2	lab	0.2	0.318	0.202	1.541	1.563	1.014
3	lab	14.2	0.388	0.234	1.789	1.842	1.030
4	lab	14.2	0.421	0.259	1.532	1.577	1.029
5	lab	14.2	0.422	0.260	1.538	1.573	1.023
6	lab	0.2	0.425	0.262	1.552	1.654	1.066
7	lab	0.2	0.505	0.300	1.774	1.906	1.074
8	lab	14.2	0.509	0.303	1.791	1.851	1.034
9	Tunnel A tank	14.2	0.389	0.234	1.789	1.824	1.020
10	Tunnel A tank	14.2	0.390	0.236	1.797	1.867	1.039

Table 3. Summary of Tunnel A Test Results

Test	M_∞	$Re_\ell \times 10^{-6}$	α, deg	W_p, gram	Impulse, lb-sec	$\bar{\theta}_p$, deg	$\bar{\theta}_m$, deg	$\frac{\bar{\theta}_m}{\bar{\theta}_p}$
11	3	12.2	1.14	0.317	0.201	1.212	1.283	1.059
12	3	12.2	0.96	0.319	0.203	1.223	1.260	1.030
13	3	12.2	0.94	0.419	0.258	1.207	1.295	1.073
14	3	12.2	0.98	0.419	0.258	1.207	1.290	1.069
15	3	12.2	2.02	0.421	0.259	1.195	1.248	1.044
16	3	12.2	3.11	0.422	0.260	1.152	1.194	1.036
17	3	12.2	3.08	0.422	0.260	1.152	1.213	1.053
18	3	12.2	4.42	0.421	0.259	1.081	1.163	1.076
19	3	23.1	2.64	0.506	0.301	1.155	1.216	1.053
20	3	23.1	2.64	0.506	0.301	1.155	1.228	1.063

$\omega d/2V_\infty$ = 0.0017 to 0.0020

NOMENCLATURE

d	Model diameter, 2.000 in.
F	Impulse force, lb
g	Acceleration of gravity, ft/sec^2
h	Vertical movement of center of gravity of ballistic pendulum system due to the impulse (see sketch A), ft
I	Model or pendulum moment of inertia about the pivot axis, slug-ft^2
k	Radius of gyration, ft
ℓ	Model length, 40.5 in.
M_∞	Free-stream Mach number
M_θ	Restoring moment parameter, ft-lb/rad
$M_{\dot{\theta}}$	Damping parameter, ft-lb-sec/rad
m	Mass of ballistic pendulum system, slugs
p	Vacuum or tunnel tank pressure, psia
p_o	Tunnel stilling chamber pressure, psia
q_∞	Free-stream dynamic pressure, psi or psf
Re_ℓ	Free-stream Reynolds number based on model length
r	Distance from the pivot to the point of action of the explosion, ft
$\bar{r}$	Distance from the pivot to the center of gravity of the ballistic pendulum system, ft
T_o	Tunnel stilling chamber temperature, °R
t	Time, sec
V_∞	Free-stream velocity, ft/sec
W	Weight of ballistic pendulum system, lb

W_p	Weight of propellant, gram
x_p	Distance from model nose to pivot axis, in.
α	Angle of attack
θ	Angular position of the model or pendulum, deg
θ_m	Measured angular position of the model, deg
$\overline{\theta}_m$	Measured model amplitude at the initial peak, deg
θ_p	Predicted angular position of the model, deg
$\overline{\theta}_p$	Predicted model amplitude at the initial peak, deg
θ'	Amplitude of the exponential envelope at t = 0 (see sketch B), deg
$\dot{\theta}$	Angular velocity of model or pendulum, rad/sec
ω	Frequency of oscillation, rad/sec

SUBSCRIPTS

0	At t = 0
1	At $t = t_1$
2	At $t = t_2$